NRSP-2
92-30

Airborne CCD-video monitoring
Performance and application of a colour infra-red video system

J.G.M. Bakker
B.M. Braam
H.J.C. van Leeuwen
R.J. de Boer

BELEIDSCOMMISSIE REMOTE SENSING

BCRS 92-30 MD

Airborne CCD-video monitoring Performance and application of a colour infra-red video system

J.G.M. Bakker
Cartoscan
B.M. Braam
Karelsilva Oy
H.J.C. van Leeuwen
Wageningen Agricultural University,
Dept. of Land Surveying and Remote Sensing
R.J. de Boer
Cartoscan

bcrs project 3.4/CO-03
bcrs report 92-30

ISBN 90 5411 075 9

August 1993

This report describes a project, carried out in the framework of the National Remote Sensing Programme (NRSP-2), under responsibility of the Netherlands Remote Sensing Board (BCRS).

CIP-GEGEVENS KONINKLIJKE BIBLIOTHEEK, DEN HAAG

Airborne

Airborne CCD-video monitoring : performance and
application of a colour infra-red video system / J.G.M.
Bakker ... [et al.]. - Delft : BCRS, Netherlands Remote
Sensing Board. - Ill. - (BCRS report ; 92-30)
BCRS project 3.4/CO-03, uitgevoerd in het kader van NRSP-2
onder verantwoordelijkheid van de Beleidscommissie Remote
Sensing (BCRS). - Met lit. opg., reg.
ISBN 90-5411-075-9
Trefw.: CCD-video / remote sensing.

CONTENTS

SUMMARY

CCD-videography may be used as a fast and inexpensive remote sensing tool. In order to perceive the radiometrical and geometrical characteristics and the efficacy of a colour infra-red CCD-video configuration, a number of crucial tests has been performed, using a Silvacam, i.e. a Finnish colour infra-red video camera, developed by Karelsilva Oy. A video cassette recorder and a 80486 personal computer with a "TARGA+" video frame digitizer board completed the video test configuration.

A professional video camera such as the Silvacam is equipped with a number of settings, which influence the radiometrical behaviour of the camera. Camera optics in particular, and its settings, determine the geometrical properties of the camera, relative to scale and angle deformation. In order to assess and verify the camera characteristics and the effects of the settings, the camera was tested indoors and outdoors, recording objects with known reflectances and specific geometrical properties. An airborne survey has been carried out, and its results compared with reflectance measurements in the field and CAESAR data.

The test results may serve as a sound basis for further development of CCD-videography into a reliable and effective remote sensing tool for the production of maps from digitized and mosaicked video frames, as an input for GIS and for monitoring purposes.

ACKNOWLEDGMENTS

The following persons and institutes are greatfully acknowledged for their support towards the succesful accomplishment of this report.

The Department of Surveying, Photogrammetry & Remote Sensing (Wageningen Agricultural University) is acknowledged for making room and equipment available for the indoor test series. Dipl.-Ing. C. Büker is thanked for the supply of radiometrical data from the CAESAR scanner, Dr. Ir. J.G.P.W. Clevers for his comments about the radiometrical aspects of the Silvacam. D.A. de Wit and D. Joghems for their support concerning the logistics.

Inter (VCD) bv is thanked for the free disposal of a conventional JVC CCD-video camera. The Dutch Remote Sensing Board (BCRS) is thanked for the use of their reflection panels.

Ir. C. Smorenburg and Ir. J.J.M. Groot Schaarsberg (TPD, Delft) are appreciated for their comments on the first draft of the report and their suggestions for the second test series.

Ir. R.W.M.E. Verhoeven is acknowledged for his support in the field and in the laboratory during the second test series.

Prof. Dr. P.D. Jungerius of the Landscape and Environmental Research Group (University of Amsterdam) is greatfully acknowledged for his enthousiastic support in the field at Schouwen and his ideas about the practical use of an airborne video system with regard to the requirements of the interpreter.

INTRODUCTION

The present research project was carried out in order to show that videography is a remote sensing tool in its own right. Like aerial photography, video remote sensing produces analog images, but unlike the former technique, these images are available right after or even during the survey flight, permitting its application in event-based operations that do not allow any delay.

Video images are stored on extremely inexpensive medium. The high rate of image refreshment (25 images per second) results in continously varying view angles of features along the flight direction. In addition, a fairly simple PC configuration permits selection and digitizing of the analog images, i.e. frame grabbing, and successive image processing. These procedures enlarge the possibility of operational applications of video remote sensing to a considerable extent.

The relatively low spectral resolution of video cameras due to the limited bandwidth and the addition of noise are their major drawback. The lack of spectral bands outside the visible region limits the value of true colour video systems for agricultural and resource applications, as opposed to colour infra-red video cameras like the Silvacam.

The Silvacam is developed and patented by Karelsilva Oy and the Instrument Technology Laboratory of the Technical Research Centre of Finland (VTT). It is a 3-CCD colour infra-red Super-VHS video camera. Silvacam's sensitivity pertains to 3 bands: green, red and infra-red.

This report deals with testing the Silvacam as an airborne remote sensing device, applicable to resource management. For the absolute radiometrical accuracy of the video camera, flights were performed over agricultural fields in the Flevopolder, the Netherlands. Other tracks were flown to evaluate the Silvacam as a remote sensing tool in event-based operations: a coastal dune area at Schouwen (in the south-western part of the Netherlands), Hulshorster Zand (a deflation area near Harderwijk), Slijkplaat (a sandbank in the Haringvliet waters) and Saeftinghe (a mud flat area along the Westerschelde). The city of Zeewolde, also in the Flevopolder area, was chosen for geometrical tests.

CHAPTER 1

DESCRIPTION OF THE VIDEO SYSTEM

1.1 Video standards

Before describing the colour infra-red (CIR) configuration, used for processing recorded video images, a brief description of some terms related to the building of analog video signals may be useful.

Up till now there are three colour television broadcast standards: NTSC (National Television Standard Committee) in the United States, SECAM (Systeme Couleur Avec Memoire) in France and some eastern European countries, and PAL (Phase Alternative Line) in western Europe. In the context of this report the PAL standard is essential.

PAL is based on the CCIR standard for monochrome video signals, which was drawn up in the late 1950's. This video signal is based on a transmission of 25 *frames* (images) per second. Each frame consists of 625 lines from which consecutively the odd-numbered and the even-numbered lines are being transmitted. This is called an *interlaced* video signal. A sub-frame, containing only the odd or even image lines, is called a *field*. The beginning of each field is indicated by a vertical synchronisation signal (vsync or field sync). Each line is marked by a line synchronisation signal (hsync or horizontal sync). The CCIR monochrome video signal or *luminance* is a combination of field information, synchronisation pulses and *blanking*, periods in which no pictorial information is transmitted.

In colour broadcasting, the image is scanned in three different spectral bands: red, green and blue (RGB). Any colour can be defined as a weighed combination of these three principal components. In order to keep colour television broadcasts compatible with black and white video, the PAL standard defines a video signal, the *composite video* signal, which is composed from the CCIR luminance (Y) and the *chrominance* (C), a signal which contains colour *hue* and *saturation*. *Hue* is the colour tint, e.g. red or yellow and is defined in degrees, where 0° is blue, 100° is red and 240° is green. The *saturation* is a quantity for the amount of white in the colour. A 100% saturated colour contains no white light, for instance deep red whereas a 0% saturated colour will be very pale (e.g. pink).

The advantage of composite video is that this is a widely used standard and has all necessary image information combined in one signal (and needs only one cable!). Mixing colour and luminance components, however, always causes interference phenomena and signal loss due to

video signal conversion to the primary RGB-signals in, for example, TV-sets. When recording video signals with a video cassette recorder (VCR) extra signal loss is caused by noise and the limited spectral bandwidth of the video tape.

Video recorders and tapes have improved a lot since the development of early video systems as VHS. Super-VHS (S-VHS) offers the possibility to access the Y and C signals separately, registers the full luminance bandwidth (5 MHz) instead of 3 MHz for normal VHS, and shows a significant increase in image lines (from 230 to 400). This results in better defined and less noisy images.

1.2 CCD-video imaging

The CCD-video technique, as applied in the Silvacam camera, is basical the same as any standard Super-VHS camera and consists of an optical part and an electrical part.

The optical part of the camera consists of lenses for focussing, a diaphragm for controlling the incoming radiant energy and a prism for splitting the incoming light in three spectral components, i.e. visible blue, green and red for conventional cameras, and green (505-580 nm), red (580-680 nm) and near infra-red (770-840 nm) for the Silvacam.

Three CCDs, one for each spectral band, register the optical information as electrical signals. A CCD consists of a matrix of 668(h) x 575(v) radiation-sensitive cells, which are electrically charged when hit by photons. After a certain exposure time, the charges are read out as voltages, the cells are neutralized and ready to be hit by photons again. The voltages read are amplified, and the responses of the three CCDs will be processed to luminance and chrominance signals (S-VHS cameras) and composite video.

The spectral sensitivity of CCD's ranges from ultra-violet to infra-red (see figure 1). In conventional video cameras the part of the desired spectrum will be filtered to direct the proper spectral information to the CCD.

1.3 White balance

In every professional video camera the *white balance* can be adjusted. The white balance is the ratio between the three basic colours for a white object under certain light conditions. The spectral characteristics of a light source changes with its *colour temperature*, which is the temperature of a black body with the same spectrum. Indoor light conditions with tungsten lamps have a colour temperature of approximately 3200 K, which means

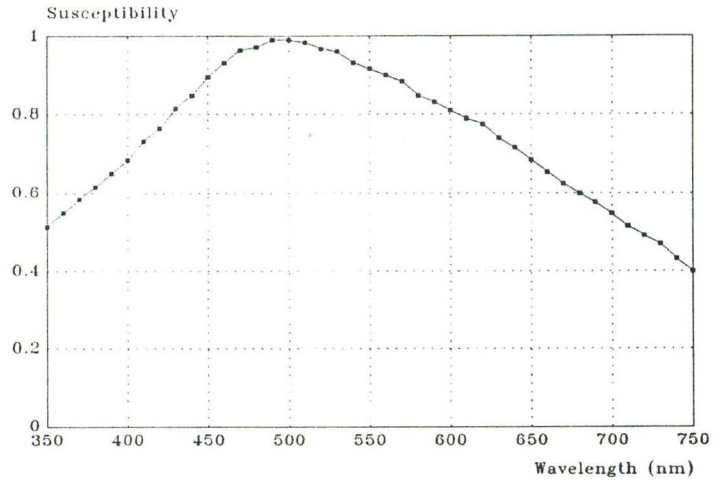

Figure 1 Spectral response of a CCD element as used in the SILVACAM video camera. (Source: Victor Company of Japan Ltd.)

that the spectral distribution of the light output is similar to that of a black body heated to 3200 K, and yields other spectral characteristics than outdoor light conditions (colour temperature at midday about 5600 K). The colour rendition is affected therefore by changing light conditions. During white balancing, the balance between blue, green and red is adjusted in such way that white objects will remain white after recording.

CHAPTER 2

VIDEO HARDWARE CONFIGURATION

The video configuration we are dealing with consists of:

- Silvacam video camera
- Super-VHS video cassette recorder
- 80486 PC with "TARGA+" videographics adapter
- Video monitor

The total video configuration as used during tests is shown in figure 2.

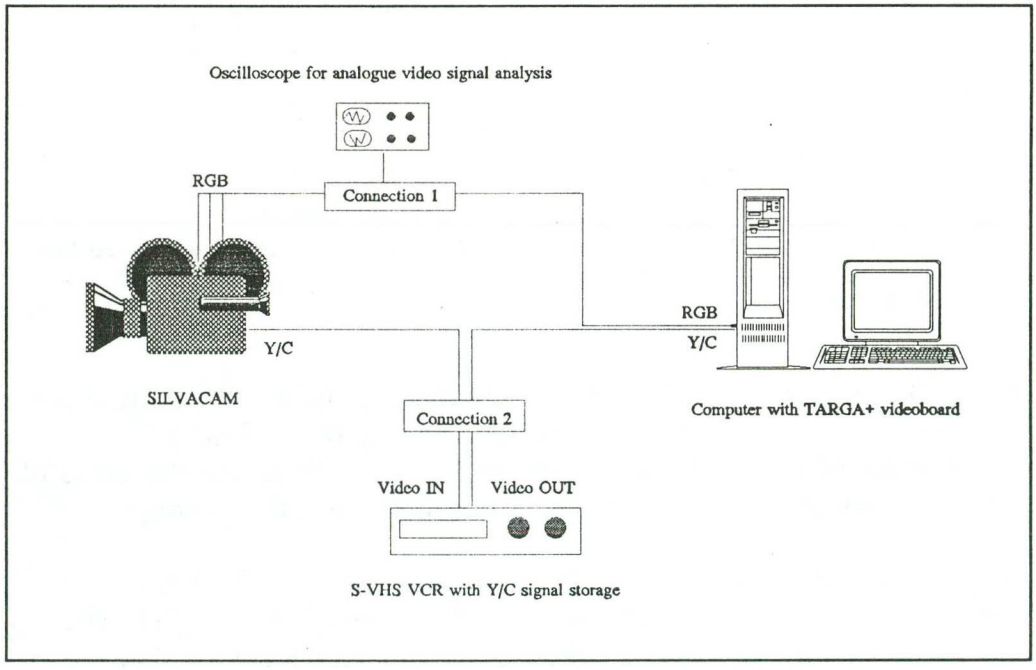

Figure 2 Line up of the video configuration.

2.1 The Silvacam camera

The Silvacam is a Super-VHS 3-CCD CIR camera and a modification of a conventional video camera, i.e. JVC's KY-FE30. The main difference between the Silvacam and a conventional camera is the spectral range: green, red and near infra-red (NIR) instead of blue, green and red. Table 1 shows the spectral ranges for the Silvacam and a conventional camera, respectively.

	SILVACAM	KY-FE30
Blue band		410-480 nm
Green band	505-580 nm	505-570 nm
Red band	580-680 nm	575-630 nm
NIR band	770-845 nm	

Table 1 Spectral range of two CCD cameras at 50% transmission.

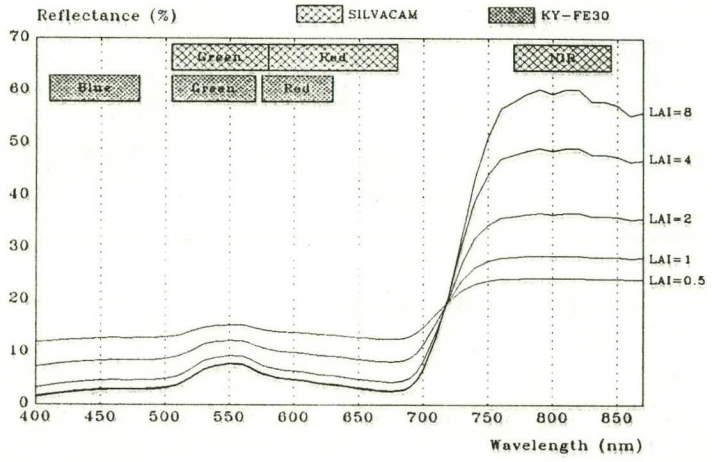

Figure 3 Spectral passbands of the SILVACAM and the KY-FE30 cameras in relation to some Leaf Area Indices (LAI) based on the SAIL model. (Source: J.G.P.W. Clevers, Agricultural University, Wageningen)

In figure 3 the passbands of the Silvacam and a conventional camera are compared with a spectral response model of vegetation (SAIL). The spectral bands of the Silvacam are situated sufficiently in the flat areas of vegetation responses to monitor vegetation with this CIR technique.

The standard lens system of the Silvacam is a customary 7-70 mm zoomlens (type HZ-410E) with iris values between f/1.4 and f/16. The Silvacam offers the possibility to choose for auto-iris, meaning that the aperture will be varied according to the amount of incoming light. This value is measured in the lower 2/3rd of the video image, as video is generally applied in the "ordinary horizontal" way of looking at the world with a bright sky at the top and darker objects in the lower part of a image. The automatic aperture control causes two serious drawbacks:

- With changing apertures the amount of incoming radiant energy changes as well. As we are yet unable to register the used aperture for each video frame, this mode cannot be used if we want to compare objects in different frames on their radiometrical content. Only objects within one video frame can be radiometrically compared.

- As the aperture is determined by the incoming amount of radiant energy in the lower 2/3rd of the screen, contrasting elements which are positioned "above" each other in the scene may lead to either blooming of highly reflecting objects if dark objects are located in the upper half of the scene or vice versa.

Due to these effects it is recommended to fly video surveys with a fixed aperture.

The shutter fixes the time that the CCDs are exposed to the incoming radiation. A combination of shutter speed and aperture of the diaphragm determines the total amount of incoming radiant energy. The Silvacam attends to four shutter speeds: 1/60, 1/250, 1/500 and 1/1000 of a second. During flight the shutter speed is very important regarding blur. Blur is caused by the movement of the camera. Two subsequent fields of one frame are recorded with a time interval of 1/50 s. With a relative air speed of 50 m/s and a shutter speed of 1/60 s, an object on the ground has moved about 1 m relative to the camera before registration by the following field. If the camera is moving sideways, this may lead to an offset between odd and even lines. If the camera moves up- or downward, smear along the edges of an object will be the result. A high shutter speed will reduce these effects. Low shutter speeds results in very unsharp images, especially in combination with large focal lengths or low flight altitudes.

During white balancing, the camera samples the CCD output signals in the centre section of the image and adapts the sensitivity of the blue and red channel gain circuits to that of the green channel. The Silvacam has a preset white balance for light conditions around a colour temperature of 5600 K ("noon daylight"). It also offers two additional settings to be stored in memory by the videographer before flight performance.

2.2 Video cassette recorder

The video recorders used were standard S-VHS recorders as described in chapter 1.

2.3 Videographics adapter

For digitizing video images (frame grabbing) a MS-DOS PC (80486, 25 MHz) with Truevision's "TARGA+" video board has been used. The "TARGA+" board can sample images at different sampling frequencies, depending on the defined spatial and radiometrical resolution. The sampling frequency can be adjusted between 9.5 and 15 MHz, meaning a sample resolution varying between 512 to 768 columns for each scan line. The number of rows varies between 476 and 576 lines. The "TARGA+"

board has a memory of 2 Mbyte, restricting the spatial and radiometrical resolution. A high spatial resolution results in a low radiometrical resolution and vice versa. An a-priori knowledge for what purpose the frame will be used is needed to select a correct graphics mode.

The "TARGA+" board offers also the possibility to grab only one field of an image. This option can be very convenient to reduce image blur due to airplane movements. A field contains either the odd or the even lines of an image. The missing lines will be acquired by taking the mean of the adjacent lines. This means that geometrical accuracy will be improved by grabbing a field but that half of the radiometrical content will be swept away.

CHAPTER 3

TEST AND CALIBRATION OF THE VIDEO CONFIGURATION

Mainly because a S-VHS video camera is not designed to perform exact radiometrical and geometrical measurements, the total video configuration from camera to grabbed image had to be tested. Tests were applied to three video components in particular:

- Video camera (conversion from optical to electrical information).
- Video cassette recorder (storage and reading of Y/C video information).
- "TARGA+" frame grabber (A/D conversion of composite video, Y/C or RGB signals).

Both indoor and outdoor tests were performed. The indoor tests took place under controlled light conditions. Several targets with known reflectances (see table 3 in chapter 4) were uniformly lighted by tungsten halogen lamps with a colour temperature of 3200 K. While the bandwidths of the Silvacam differ from those of the KY-FE30 (see table 1), the reflectance characteristics of the targets differ as well. A series of different reference panels and a calibrated grey tone chart were used as targets for the radiometrical calibration. A millimetre grid chart has been used for geometrical tests. Both video cameras were used.

For the outdoor tests several tracks in the Flevopolder were flown with the Silvacam camera. The first outdoor session was in July 1991, the second one in June 1992. During the flights, three BCRS reflection panels were used as reference targets, to obtain the reflectance characteristics of some agricultural fields. Also field measurements with a cropscan meter were carried out. This cropscan meter yields reflectance percentages in 8 small passbands between 490 nm and 1090 nm. The village of Zeewolde was chosen for geometrical measurements.

During the first outdoor test series, there happened to be problems with the white balance setting of the Silvacam. At that time an alternative was chosen in that the white balance procedure was carried out in the air. As we will see from the test results, this procedure had important consequences for the mutual relation between the three video channels, and consequently on the indoor as well as on the outdoor results. In September 1991 it was decided to perform indoor tests with a conventional RGB CCD-camera to try and tackle the problem. The results of these tests revealed insight in the technical aspects of the camera, such that they served as a basis for a revision of the Silvacam, that lead to a second series of tests in June 1992 (test 2).

In this report we will concentrate on the most recent test results with the Silvacam (test 2). Where required, we will also use older test results either with the Silvacam (test 1) or with the JVC KY-FE30 camera.

3.1 Camera tests

The camera rests included the following aspects:

- Linearity of CCDs.
- Influence of white balance setting on the radiometrical range.
- Light fall-off of the optical system versus focal length.
- Influence of different light intensities by using neutral density filters.
- Influence of diaphragm and shutter settings.

3.2 VCR tests

The use of a storage medium and reading device may lead to radiometrical distortion of the original Y/C video signal. Therefore the following items were tested:

- Influence of tape storage on the video signal and the type of VCR equipment used. Both tests were performed with results obtained during test 1 with the Silvacam. Despite the erroneous white balance setting at that time, the results are considered illustrative for the effect of tape and VCR on the stored video frames.

- Influence of type of VCR.
  Two different types of S-VHS VCRs were used to read out the tape-stored Y/C signal:

  - The Panasonic AG-7330; a professional S-VHS VCR.
  - The JVC HR-S5500E; a semi-professional S-VHS VCR.

3.3 A/D conversion tests

The "TARGA+" board was tested by grabbing images of objects with known reflection characteristics. The A/D conversion was tested in different graphical modes:

- Low spatial resolution (512(h) x 576(v) pixels), high radiometrical resolution (32 bits)
- High spatial resolution (768(h) x 576(v) pixels), low radiometrical resolution (16 bits)

- Same as above with different contrast and saturation settings of the "TARGA+" board.

CHAPTER 4

RADIOMETRICAL PROPERTIES OF THE VIDEO CONFIGURATION

4.1 Linearity of the CCDs and video board

The relation between the reflectance of an object (r_o) and the amount of radiant energy, as detected within a single passband, by the CCD elements (Q_{CCD}), may be assumed to be a linear one, when recordings are performed under similar atmospheric conditions, and when certain properties of the camera like light fall-off, focal setting etcetera, are accounted for, and, if necessary, corrected for (Slater, 1980; Clevers, 1986).

The linear equation, describing the relation between the reflectance of an object and the detected radiant energy, is then:

$$r_o = a + b * Q_{CCD}$$

where a and b are constants, whose values depend on the wavelength of the light in the passband.

From the equation it is clear that such linearity can only be detected by the user, if the instruments - in our case the camera and the video board - contain linear converters (CCDs and A/D converter respectively). This means that for the purpose, the conversion of the incoming radiant energy to an electronic video signal should be linear, as well as the A/D conversion on the video board.

Grey tone number	Reflectance (%)
1	63
2	57
3	51
4	45
5	39
6	33
7	27
8	21
9	15
10	9
11	3

Table 2 Reflectances of the grey scale chart bars.

In order to test conversion linearity, a chart made up of 11 grey bars, varying from black to white with known reflectances (table 2), was recorded by the Silvacam, under uniform indoor light conditions, and after a proper white balance setting (see 4.2). The diaphragm was fixed at f/5.6,

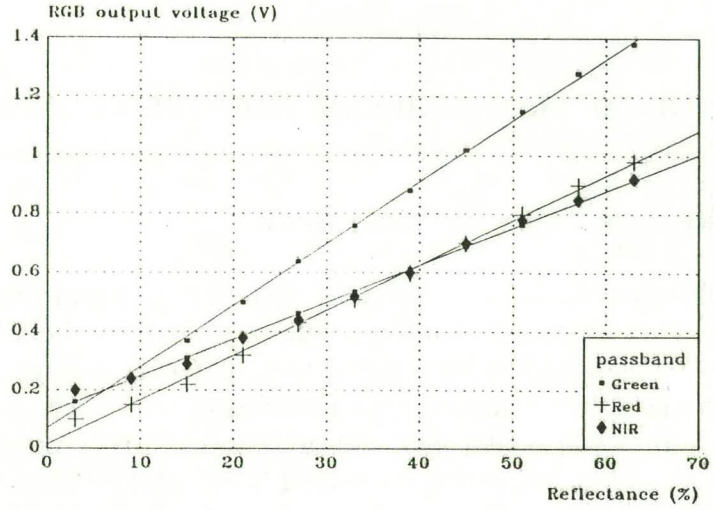

Figure 4 Relation between input reflectance and SILVACAM output voltages for grey tone chart.

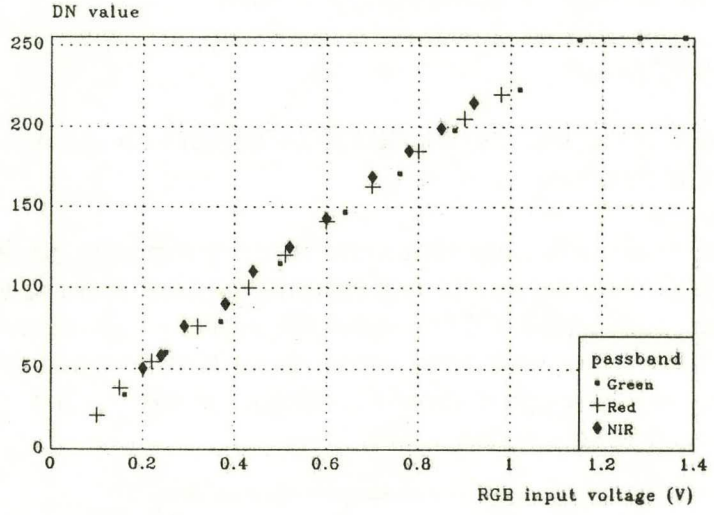

Figure 5 Relation between SILVACAM output voltages and DN values of grabbed image of grey tone chart.

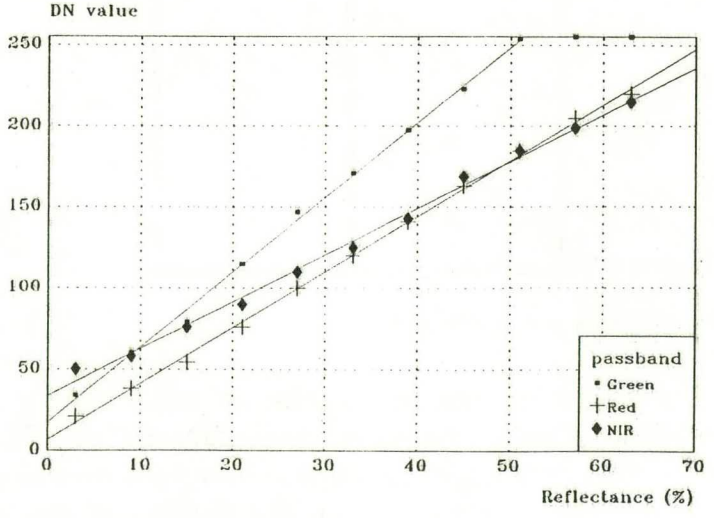

Figure 6 Relation between grey tone chart reflectance and DN values of grabbed image for the SILVACAM.

with f=30 mm and a shutter speed of 1/60 s.

CCD linearity was tested by reading out the RGB voltages of the grey bars with an oscilloscope. If the CCD elements are indeed linear converters, it must be possible to describe the relation between the reflectance values of a bar and the generated analog video signal by a linear regression model, for each of the three channels. As we see from figure 4, the relations between reflectances and RGB output voltages is sufficiently linear for each of the passbands.

The response of the video board has been verified in the highest possible radiometrical resolution mode (8 bits per colour plane). The linearity of the video board is then assessed by comparing the digital numbers (DN values) of the digitized image with the analog input voltages as measured by the oscilloscope. Figure 5 shows the linearity of the A/D conversion process, which can also be satisfactorily described by a linear model for all three passbands, except for saturation effects in the green passband at high input voltages.

This means that the relation between the reflectance of an object and the resulting DN value in the grabbed image can be described by the following linear relations, as illustrated in figure 6:

$$DN_{GREEN} = 17.6083 + 4.6194 * Q_{GREEN}$$
$$DN_{RED} = 6.7227 + 3.4409 * Q_{RED}$$
$$DN_{NIR} = 33.7409 + 2.8894 * Q_{NIR}$$

4.2 White balance

The white balance adjusts the camera colour settings to the prevailing light conditions. White balancing is done by placing a grey-toned (or preferably white) object in front of the camera and pressing the auto-white-balance button. Grey-toned objects cause an equivalent amount of incoming radiant energy over a wide spectral range. If the CCD outputs for these signals differ - for instance due to changing light conditions effecting the colour temperature - the camera corrects the colour balance circuit in such a way, that the blue and red channel voltages coincide with the green channel value. This means that the green channel is used to verify the balance circuit between the three channels and, if necessary, makes corrections for the prevailing light conditions.

During the 1991 test performance (test 1), it was found that the Silvacam could not be properly white balanced. As an alternative, the white balancing procedure was carried out while flying over an unspecified area.

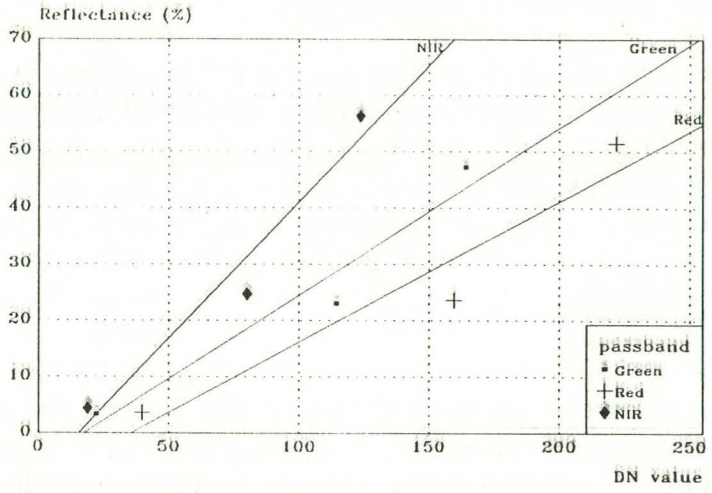

Figure 7 Video system response when white balance was set flying over an unspecified vegetated area. Objects: BCRS panels. Camera: SILVACAM. (Test 1).

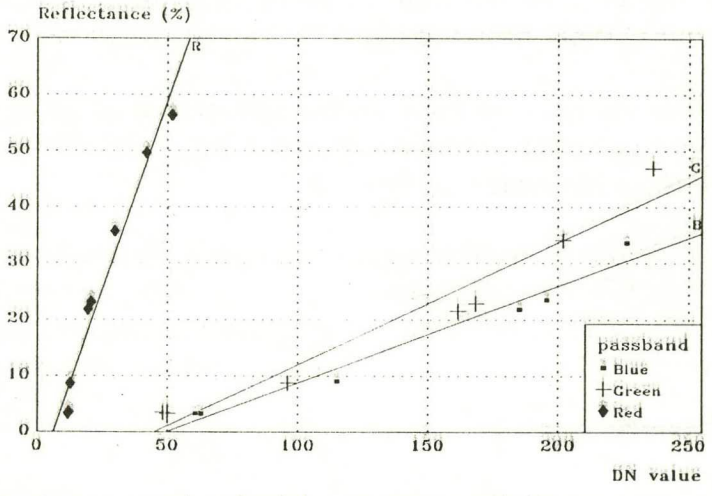

Figure 8 Video system response when white balance was set on a red object. Objects: BCRS and LMK panels. Camera: JVC KY-FE30.

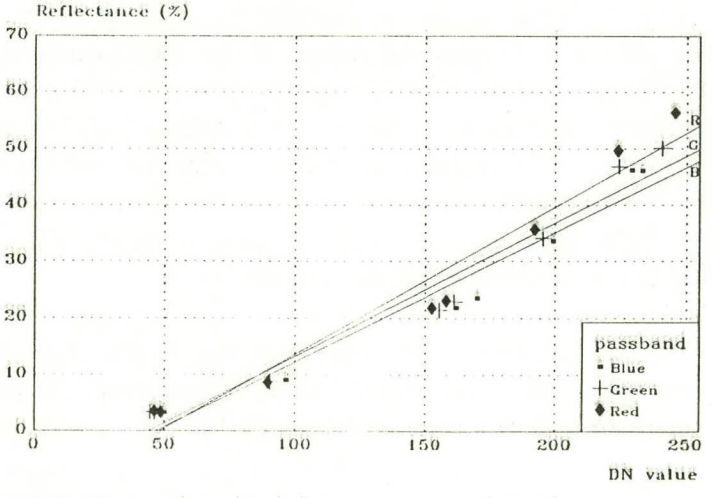

Figure 9 Video system response when white balance was set on a white object. Objects: BCRS and LMK panels. Camera: JVC KY-FE30. (Test 2).

Object	Reflectance (%)		
	Green band	Red band	NIR band
BCRS black	3.3-3.4	3.4-3.8	4.4-4.5
BCRS grey	22.8-23.2	22.8-24.3	24.5-24.8
BCRS white	46.3-48.2	48.2-54.7	56.1-56.4
LMK black	3.2	3.2-3.5	3.8-4.1
LMK dark grey	8.5-8.8	8.5-9.0	9.2-9.4
LMK grey	21.5-21.6	21.5-23.0	23.1-23.2
LMK light grey	33.7-34.8	34.8-38.5	38.3-38.5
LMK white	47.5-53.8	53.8-64.9	66.7-67.3
Blue cloth	2.8-7.3	2.8-3.5	7.0-14.4
Green cloth	8.4-22.1	8.4-9.8	25.8-51.8
Red cloth	4.6-8.7	8.7-33.4	57.2-59.8

Table 3 Reflectances of objects used for radiometric calibration of the SILVACAM.

After the said white balancing procedure, three separate grey-toned BCRS reference panels (see table 3) were recorded under controlled indoor light conditions, with an iris setting of f/11, a focal length of 50 mm, and a shutter speed of 1/60 s. The reflectances of the panels were plotted against the mean DN value (see figure 7).

When a white balance has been properly set, one may expect similar linear relations between reflectances and video sytem responses. As we see in figure 7, this is not the case. Compared to the red passband (reference channel), both the green and the NIR passband show low susceptibility to the amount of incoming radiant energy.

When flying over a vegetated area, the Silvacam will receive a high amount of radiant energy in the NIR passband, when compared to the red and green passbands. The reflectance values for green vegetation will be approximately 10% (green band), 3% (red band) and 60% (NIR band). Thus, the radiances in the green and NIR passbands are relatively high, to the effect that the gain in these channels of the colour balance circuit will be lowered, compared to the red signal, thus reducing the dynamic range of the former two passbands.

In order to test the above theory and to understand the effect of the white balance procedure in the balance circuit, a conventional RGB CCD-video camera (JVC, type KY-FE30) was tested. First the same white balance procedure as for the Silvacam was simulated by placing a red cloth in front of the lens, to the effect that the red channel received a high amount of incoming radiant energy, when compared to the other two channels. Then, with iris set at f/8, the BCRS reference panels were recorded by the camera and frames grabbed by the video board, following the same procedure as described earlier. Linear regression modelling describe the

relation between the DN values and the respective reflectance values of each panel. As it turns out, figure 8 shows a similar effect as figure 7, depicting the Silvacam response. White balancing on a red-coloured object makes the red channel very unsusceptible to variations in incoming radiant energy, i.e. reduces its dynamic range.

Figure 9 shows the JVC camera's response to a number of reference panels (BCRS and LMK, see table 3) after a correct white balance procedure has been performed. The linear relations between panel reflectance and DN values nearly coincide.

4.3 Light fall-off

Light fall-off is the phenomenon of a decrease in illumination of the CCD array with increasing distance from its centre as a result of lens properties. The effect varies with the focal length and the aperture of the lens (Lillesand & Kiefer, 1979). The conventional RGB video camera used in this project, as well as the Silvacam, has a 1/2 inch CCD facetplate (6.4 x 4.8 mm), resulting in a maximum distance of 4.0 mm (1/2 diagonal). Some light fall-off characteristics of the zoomlens used in the true colour camera, according to the manufacturer, are shown in figure 10. The incoming radiant energy in the centre is scaled 100%. The offset in the corner of the facetplate is in the order of 60% at f=97.5 mm and an iris setting of f/1.4. The offset is largely determined by the aperture used and the focal length. By using small apertures, i.e. iris < f/5.6, light fall-off may be considerably reduced. Vignetting, caused by shadowing from surfaces within the camara, generally intensifies fall-off effects, but is not considered in the tests below as a separate phenomenon. It is, however, partly responsible for the effects as measured in these tests.

The light fall-off in the Silvacam was tested by recording uniformly-lighted reflection panels, which have uniform reflectance characteristics. The panels were recorded at different focal lengths (30, 50 and 70 mm) and diaphragm settings (f/1.4, f/2.8 and f/5.6). In the absence of light fall-off, each CCD element would be expected to receive the same amount of incoming radiant energy. To register light fall-off, the video frames were grabbed and the mean DN values of 11 sample blocks along the half diagonal of the image (centre to upper left) were determined. These mean DN values were plotted against the distance from the centre in pixel units. As a frame measures 512 x 576 pixels, the length of half the diagonal will be 385 pixels. If the electronical circuit of the Silvacam does not account for light fall-off, we may expect a similar characteristic as shown in figure 10. The test results are shown in figures 11.1 through to 11.3. Figure 12 shows a three-dimensional view of the spatial light distribution in a lens.

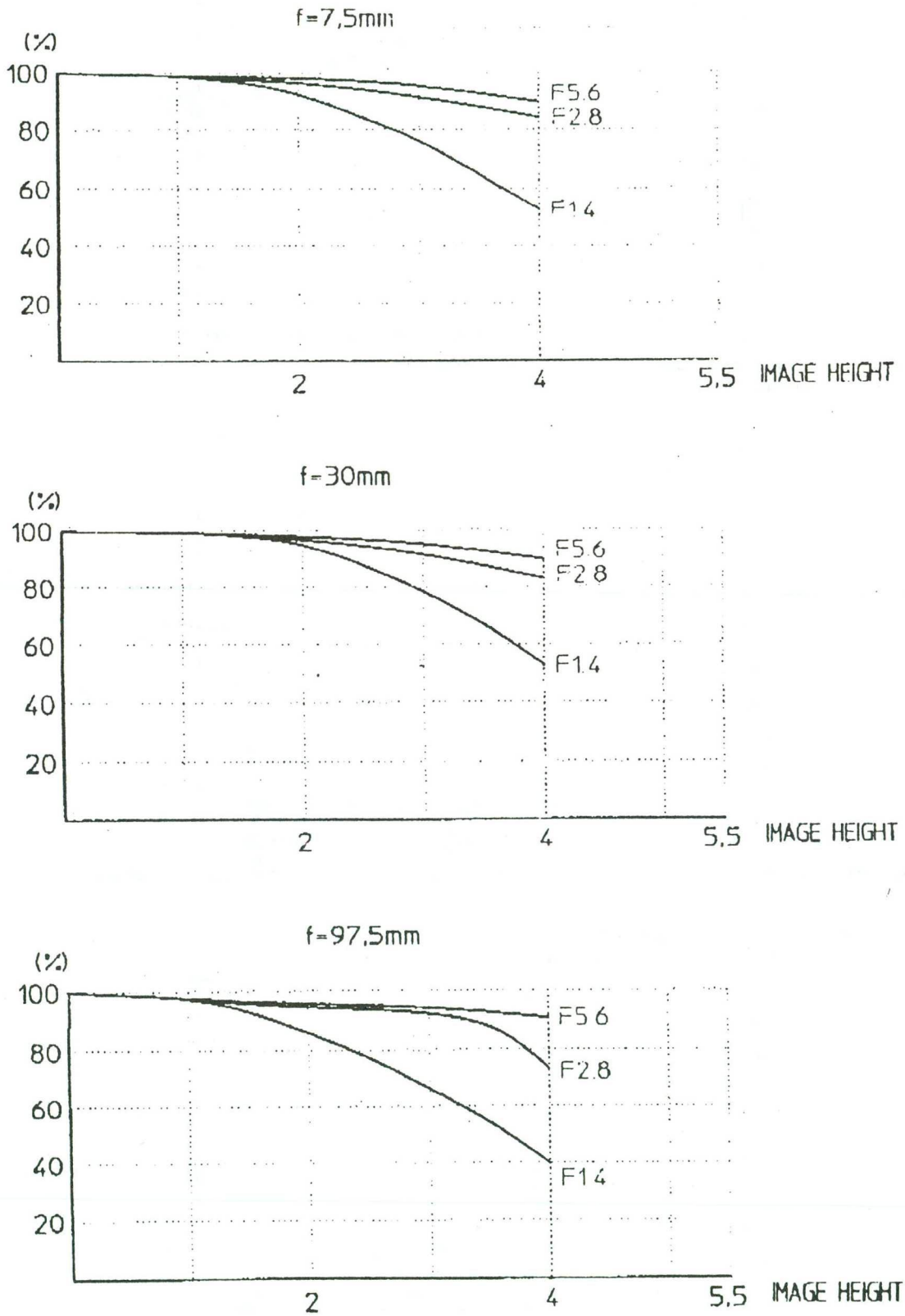

Figure 10 Light fall-off for different focal distances and iris settings of the HZ-713 zoom lens as used in the JVC KY-FE30 camera.

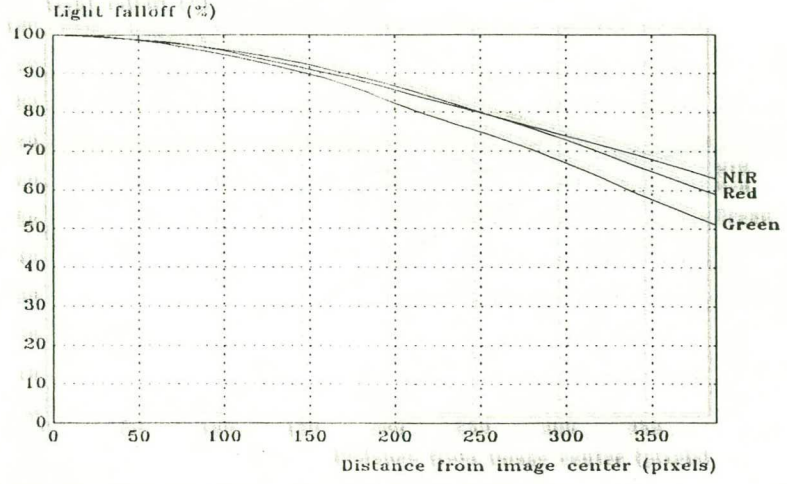

Figure 11.1 Light fall-off as function of the passband. f = 70 mm; iris = f/1.4. Camera: SILVACAM.

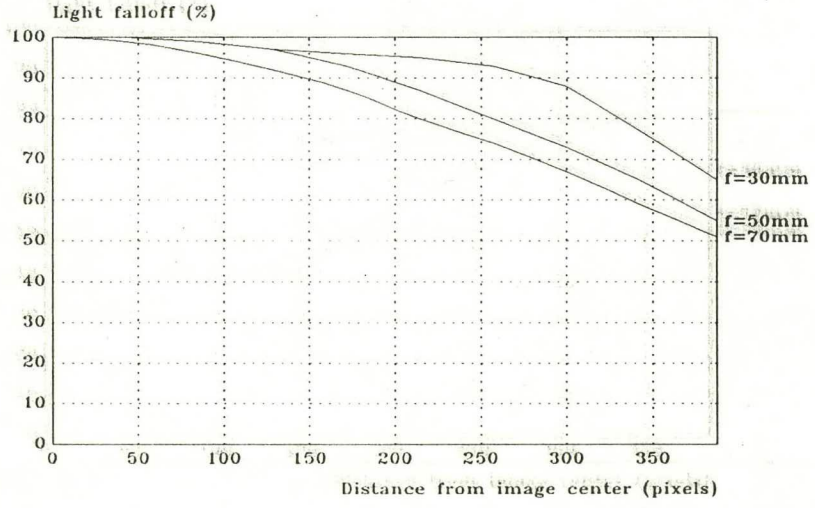

Figure 11.2 Light fall-off as function of the focal length. Green passband; iris = f/1.4. Camera: SILVACAM.

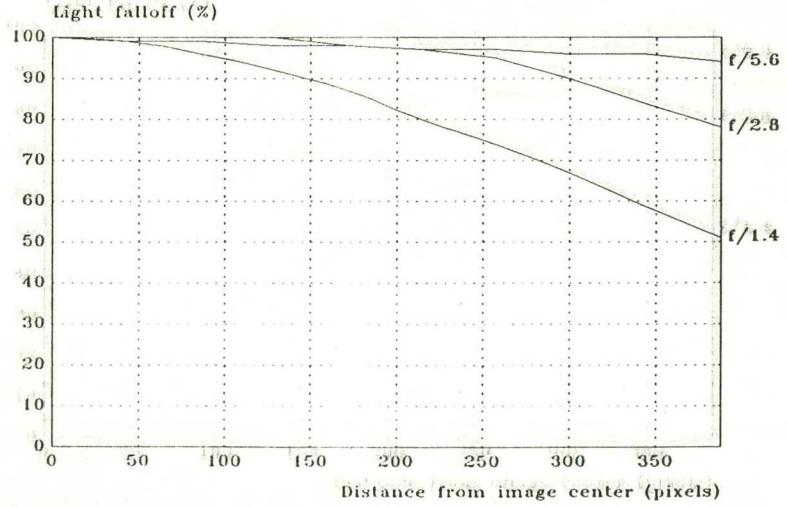

Figure 11.3 Light fall-off as function of the iris setting. Green passband; f = 70 mm. Camera: SILVACAM.

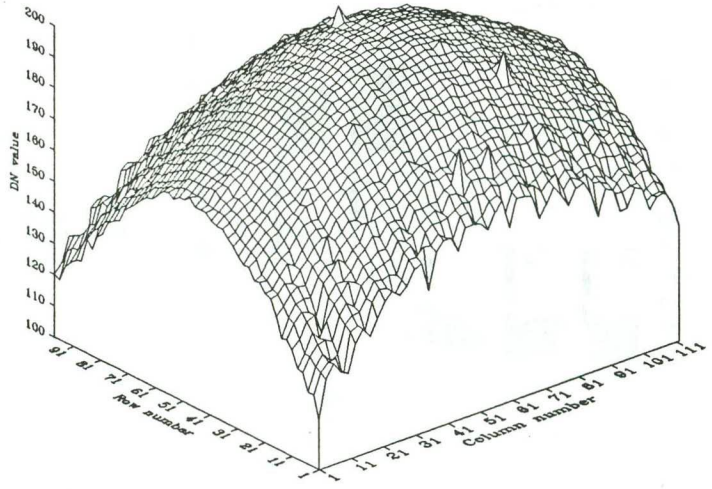

Figure 12 Light fall-off for a recorded, uniformly illuminated, reflection panel. Green passband; f=70 mm; iris=f/1.4. Camera: SILVACAM.

In the Silvacam indeed, light fall-off is not corrected for. In all three passbands, it is largely determined by the aperture and, to a lesser degree, by the focal length. Light fall-off might cause a radial decrease of circa 50% at a focal length of f=70 mm, combined with a maximum aperture of f/1.4. Apertures smaller than f/5.6 appear to cause a less-than-10% light fall-off. There are small differences in the degree of light fall-off for the three passbands.

4.4 Iris setting

When recording the same object under identical light conditions, a change in the aperture of one stop either doubles or halves the amount of incoming light. The relation between the used iris setting and the percentage changes in DN values were tested for the conventional video camera.

After a proper white balance was set, the white and black LMK panels were recorded indoors with three different f-stops (f/8, f/11 and f/16, respectively) at a focal length of 50 mm. Under these circumstances, the effect of light fall-off is assumed to be less then 5% and therefore negligible. The f-stops were set as accurately as possible. The frames were grabbed and the mean DN values for each frame and each passband were assessed.

When f/11 is taken as a reference, one would expect a 50% increase of DN at f/8 and a 50% decrease at f/16. Figure 13 shows that no such simple linear relation exists. Recording the white LMK reference panel at f/16 results in the DN values decreasing some 25%. From changing the diaphragm to f/8 follows an increase of DN values of about 35%.

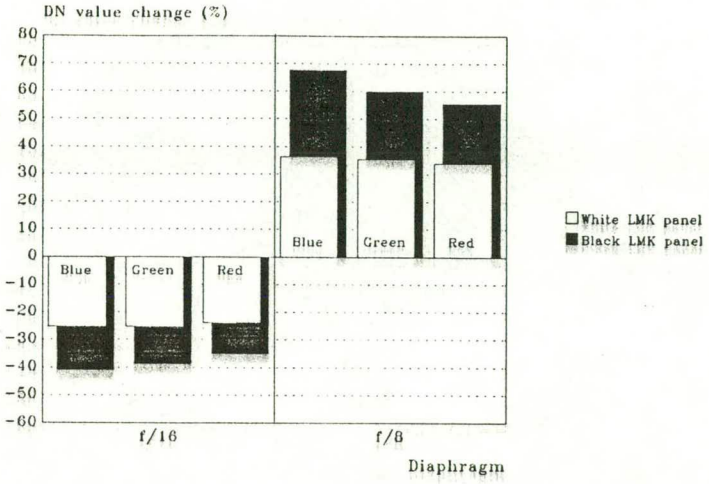

Figure 13 Relative video system response to an one f-stop change from diaphragm f/11. Camera: JVC KY-FE30.

Recording the low reflecting black LMK reference panel results in differences of about -40% and +60% respectively. An explanation for this behaviour may well be found in inaccurate aperture settings. Any deviation from the right setting will result in an quadratic abberation of incoming radiant energy.

4.5 Shutter speed

Four different shutter speeds can be selected on the Silvacam: 1/60, 1/250, 1/500 and 1/1000 of a second. From the prior condition of registering objects with a fixed aperture, varying light conditions may be such that changing shutter speed is imperative. It would therefore be of interest to know whether linearity exists between shutter speed and the amount of incoming radiant energy. If so, we will be able to fly tracks and make recordings with different shutter speeds and, in image processing, correct for the shutter speed afterwards.

In an indoor test, a white LMK panel was recorded with f=30 mm and f/3. With these settings, one has to consider a light fall-off up to 10%. The DN values of images, taken with shutter speeds 1/250, 1/500 and 1/1000 s, were compared. A supposed linearity between shutter speed and the incoming amount of energy would result in DN values decreasing to 50% and 25% respectively, when halving the shutter speed once or twice.

Figure 14 shows that halving the shutter speed from 1/250 to 1/500 s results in a decrease of DN values to 70% of the former values. A shutter speed of 1/1000 s shows DN values decreasing to 45% of the reference value.

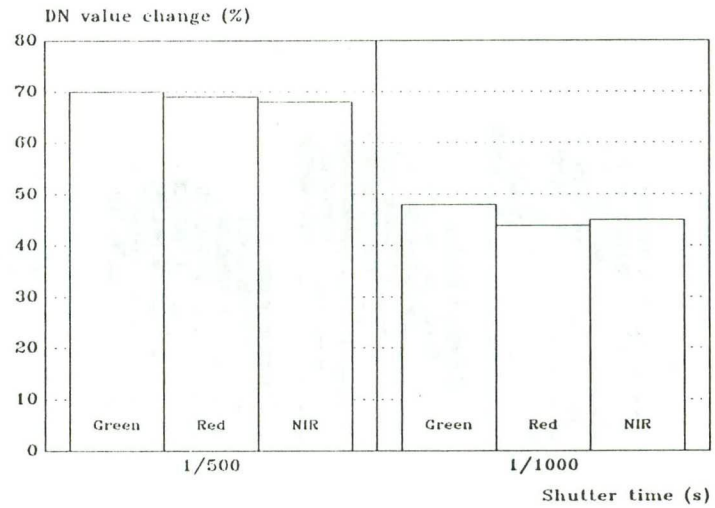

Figure 14 Relative video system response to change in shutter speed from 1/250 s. Camera: SILVACAM.

From these results one is tempted to conclude to a linear decrease of 30% as a consequence of halving the shutter speed. However, from the previous and the next test follows that the decrease of DN values depends on the reflectance of the recorded object: dark coloured objects cause a relatively sharper decline in DN values than light coloured ones.

4.6 Light reduction by neutral density filters

The use of a neutral density filter (ND filter) yields basically the same effect, in reducing the amount of incoming light with a certain factor, as choosing for a faster shutter speed or a smaller diaphragm. When operating with a fixed aperture, the use of a ND filter may solve the problem of overexposure during flight performance. It is therefore of interest to consider the relation between the nature of certain ND filters and the corresponding DN values.

Neutral density filters ND2 and ND4 reduce the incoming light intensity with 50% and 75% respectively. In the indoor test, the grey tone chart (see 4.1) was used as the recorded object. The camera was set at f=30 mm, iris f/5.6 and shutter speed 1/60 s.

Figure 15 shows relative DN values (no filter = 100%) for the eight lighter bars of the chart (numbers 1 through 8) in each of the passbands. A low signal-noise ratio prevented DN values for the darkest grey tone bars (9 through to 12) to be measured. First, it appears that, for both filters, the filtering effect is smaller for light than for dark objects. Secondly, the filtering is passband dependent, smallest in the green passband and strongest in the NIR passband.

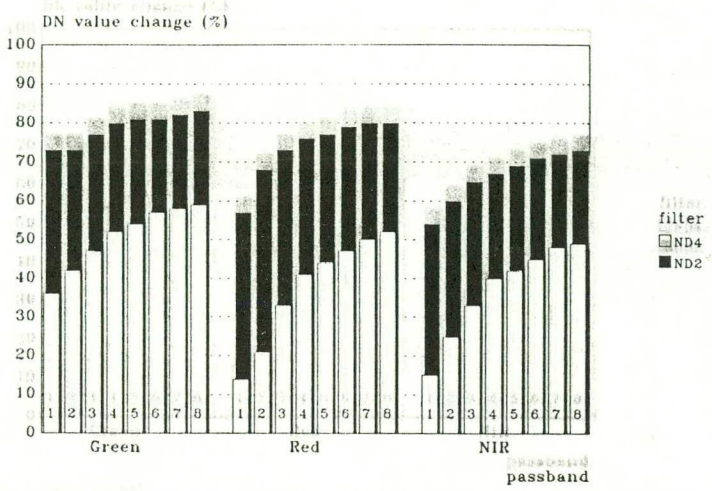

Figure 15 Relative video system response to light reduction by neutral density filters, compared to unfiltered light input. Object: grey tone chart. Camera: SILVACAM.

4.7 Tape storage

During the previous indoor tests, the Silvacam was directly connected to the "TARGA+" video board. Thus, the incoming Y/C signal was immediately digitized and stored on the PC's hard disk. In airborne videography however, one has to store the analog Y/C signal on video tape, to be grabbed later. In the present test, the influence of tape storage was determined by comparing the Y/C signal coming directly from the camera with the stored Y/C signal. The focal length was set to 50 mm. An iris setting of f/11 was chosen to minimize the effect of light fall-off. The recorded targets were three BCRS reference panels. The recorded frames were retrieved from a professional S-VHS VCR (Panasonic, type AG-7330).

The difference between directly grabbed and tape-stored images is illustrated in figure 16. It appears that, once a video image has been stored on tape, the digitized frame shows higher DN values than the frame from the non-recorded image. The relative increase of the DN values is largest for the red passband, but a similar effect shows for both the other passbands. DN values of about 240, when read out from the video camera, will yield saturated values, once the relative images have been stored on tape. An upper level of about 200 DN is therefore to be recommended. The differences between the dynamic ranges of the passbands is caused by an erroneous white balance.

The images that were used for the tape storage test, were occasionally read out from both VCRs (see 3.2) and subsequently grabbed. The corresponding models representing the relation between reflection percentages and DN values are depicted in figure 17, showing a

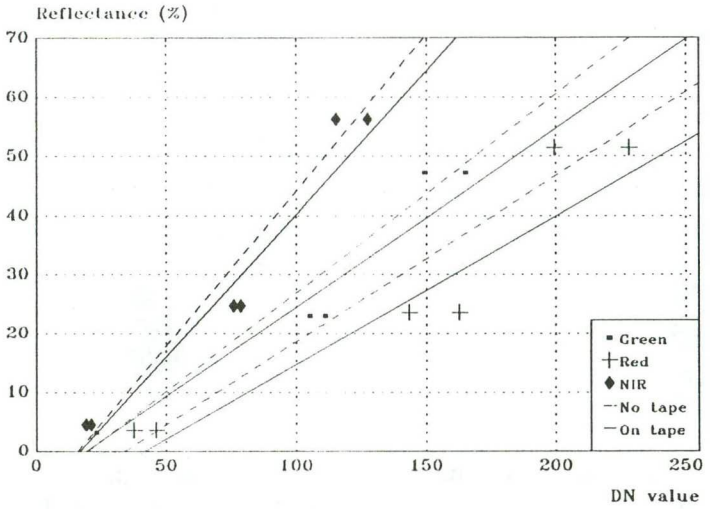

Figure 16 Video system response for tape- and non-tape-stored data. Objects: BCRS panels.

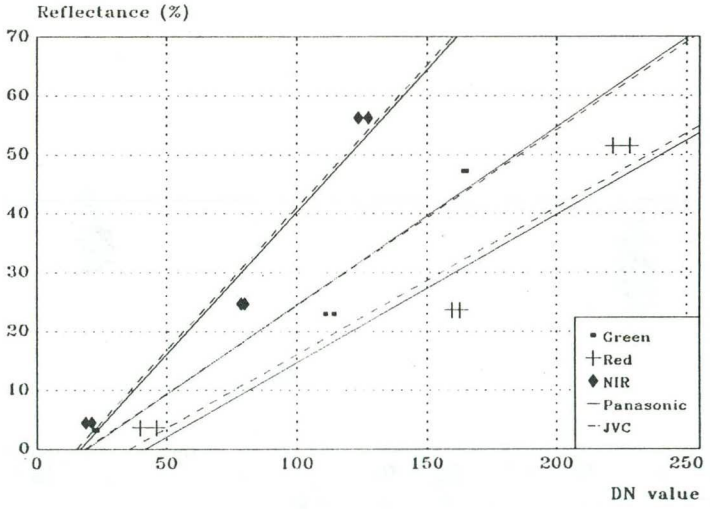

Figure 17 Video system response for two different VCR's. Objects: BCRS panels.

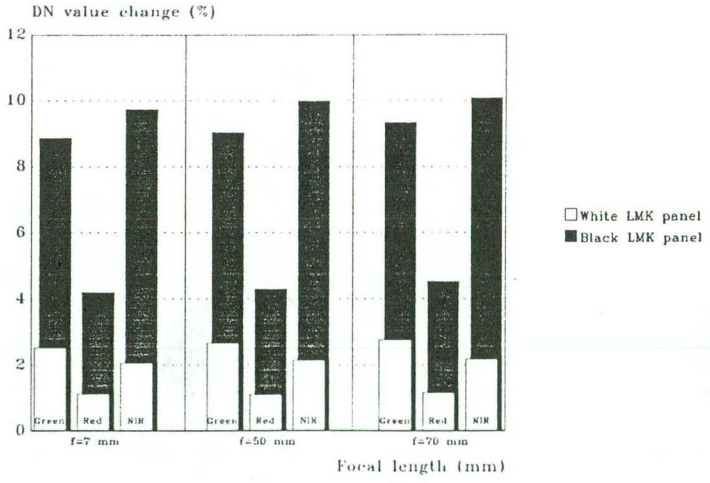

Figure 18 Variance of tape-stored data compared to non-tape-stored data for two reflection panels in three parts of the grabbed image.

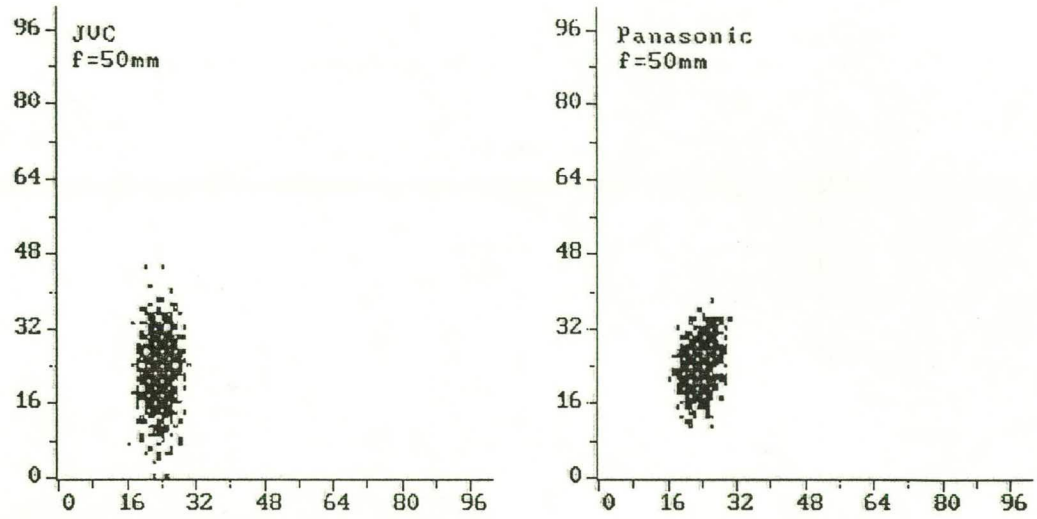

Figure 19.1 Comparision of non-tape-stored (X) and tape-stored (Y) data for two VCRs. Green passband, black reference panel.

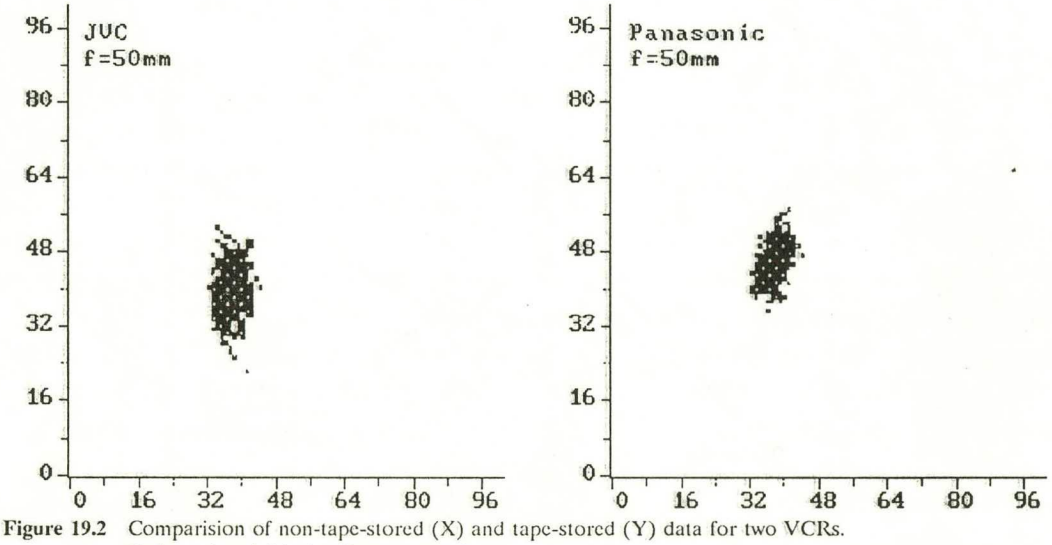

Figure 19.2 Comparision of non-tape-stored (X) and tape-stored (Y) data for two VCRs. Red passband, black reference panel.

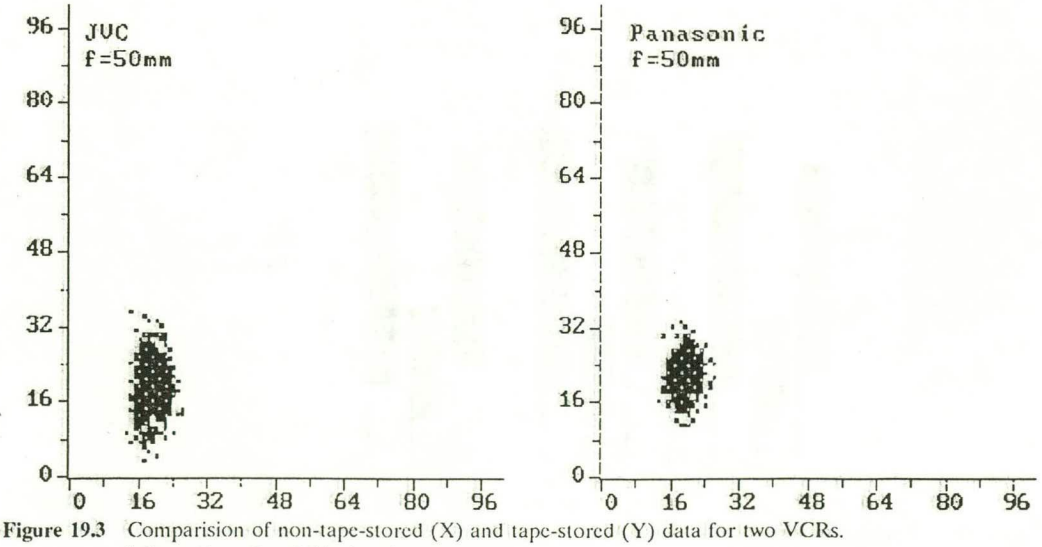

Figure 19.3 Comparision of non-tape-stored (X) and tape-stored (Y) data for two VCRs. Infra-red passband, black reference panel.

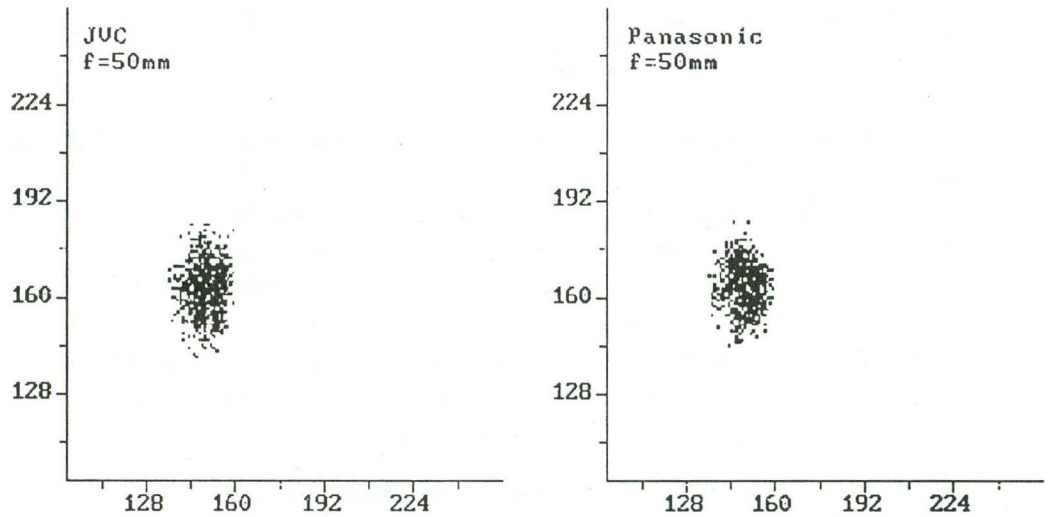

Figure 20.1 Comparision of non-tape-stored (X) and tape-stored (Y) data for two VCRs. Green passband, white reference panel.

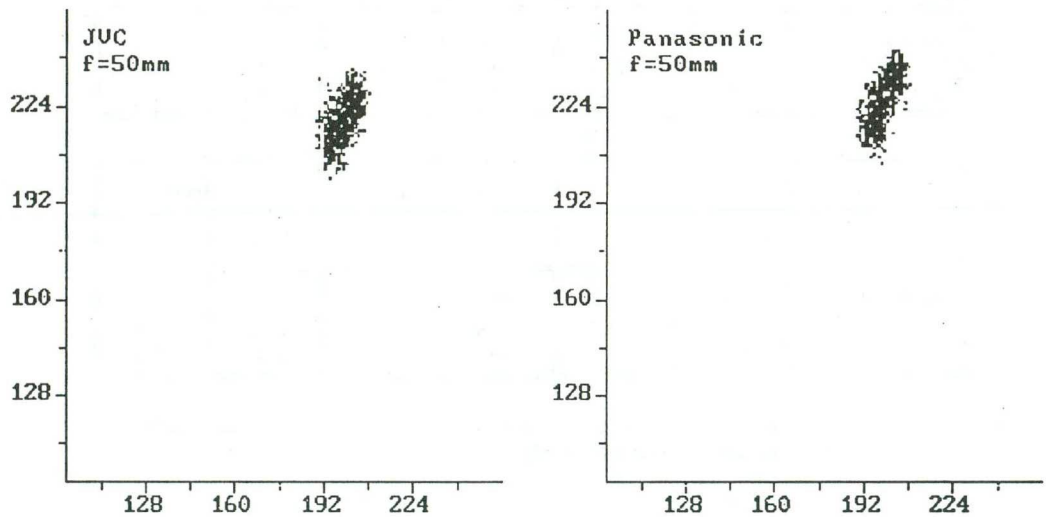

Figure 20.2 Comparision of non-tape-stored (X) and tape-stored (Y) data for two VCRs. Red passband, white reference panel.

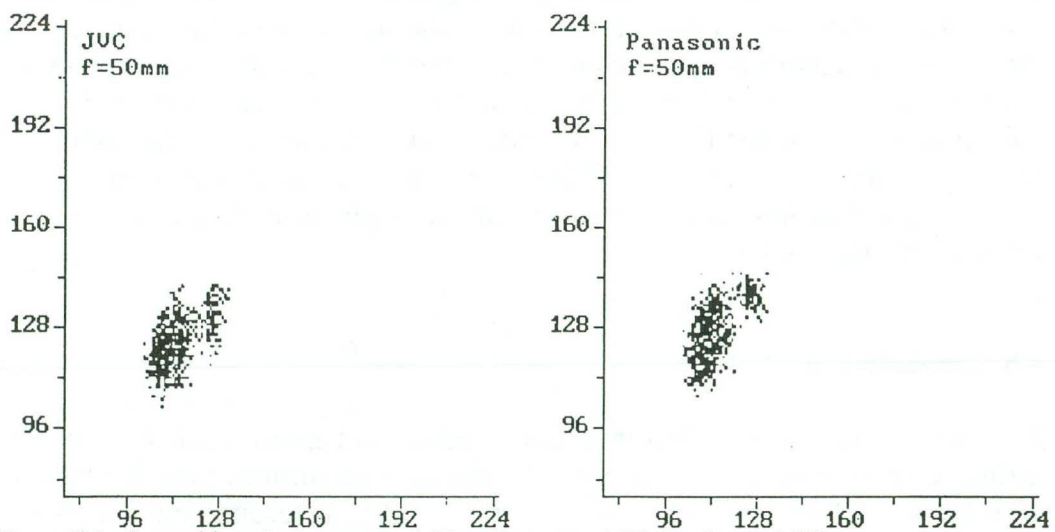

Figure 20.3 Comparision of non-tape-stored (X) and tape-stored (Y) data for two VCRs. Infra-red passband, white reference panel.

considerable similarity. Figure 18 shows the variance of DN values of grabbed frames from tape-stored data.

The influence of the VCR on the radiometrical distribution is substantial: whereas the mean DN value of an image is not effected by the VCR (figure 17), the DN range of tape-stored images can be three times as high compared to non-tape-stored images (figure 18). The radiometrical distribution also depends on the recorded target: the white reference panel shows less variance than the black one. The higher variance for low-reflecting objects can be ascribed to the influence of noise phenomena, as the *dark current* of the camera (i.e. the camera noise current in the absence of light) or tape noise when stored on tape.

Black panel	Green band		Red band		NIR band	
	Mean	Var(%)	Mean	Var(%)	Mean	Var(%)
No VCR	23.1	9.8	37.4	5.1	19.2	10.4
Panasonic	23.5	18.5	45.3	6.6	21.6	16.4
JVC	22.3	34.2	39.4	10.8	19.2	25.7

White panel	Green band		Red band		NIR band	
	Mean	Var(%)	Mean	Var(%)	Mean	Var(%)
No VCR	148.8	2.8	198.8	1.7	114.1	4.4
Panasonic	165.2	4.7	226.0	2.2	127.5	6.8
JVC	164.5	4.5	219.4	2.3	124.1	5.2

Table 4 Mean DN and percentual variation of tape-recorded and non-tape-recorded data for a black (upper table) and a white reference panel.

Figures 19 and 20 show radiometrical scattering, caused by tape storage, for two different VCRs. The corresponding means and standard deviations are given in table 4. As can be seen from the figures and the statistics, the mean values remain nearly the same, but the standard deviation shows a wide range of values, indicated by the width of the scatter plots. This variation is highest for the JVC recorder and increases when the black reference panel is considered. This effect can enhance cluster overlap when a classification on a tape-stored image is performed, specially for low-performing VCRs.

4.8 Outdoor tests

The determination of reflectance characteristics of ground objects with an airborne remote sensing system yields quantitative information. If objects with known reflectance characteristics are used as reference on the ground one can determine absolute reflectance characteristics of objects from the

air. This absolute radiometrical information of objects may be useful in agricultural field studies like monitoring plant growth, disease detection and the determination of other vegetation characteristics.

4.8.1 First test series

On the 10th of July 1991, several tracks were flown over the Flevopolder with two Silvacam cameras: one forward-looking (grazing angle about 70°) and one down-looking. The forward-looking mode was introduced to compare the vegetation reflectances with CAESAR data, as obtained on July 4th previously. The CAESAR scanner has similar, but narrower passbands as the Silvacam.

The white balance of the Silvacam was set during a flight, with unspecified vegetation as a reference. As a consequence of this procedure, the mutual relation between the three video channels was disturbed (paragraph 4.2). However, it is assumed that within each single channel, data are comparable. Therefore, a few comments on the results will be made. Images made from a flying height of 1500 ft, using a focal length of 7 mm, were found to be most convenient for the purpose. This way, the video frames cover an area of about 425 x 316 m, while ground resolution is about 60 x 60 cm.

During the test flights, the video signal was stored on tape, using a JVC camcorder which was attached to the Silvacam. Three BCRS reflection panels were used as reference targets for radiometrical calibration. In the field, crop reflectances in 8 narrow passbands (490 to 1090 nm) were obtained, using a handheld spectrometer.

4.8.1.1 Downward-looking mode

When analysing of the video frames, it appeared that large parts of the frames were saturated, including the white and occasionally even the grey reflection panels. Therefore, a few homogenous agricultural fields were chosen to be used as references. The linear models are given in table 5 and depicted in figure 21. A statistical test ("f-test") was performed to check whether a linear model fits with other data or not. If the f-value is below a critical value, the fit is rejected. The critical value for a 5% significance level is 161.4. Except for the NIR passband, the linear models are not reliable. This can partly be ascribed to the very small dynamic range on which these models are based. Notwithstanding the unreliablity of the models, the reflectance characteristics were calculated for some cultivates (table 5). When the results obtained with the Silvacam are compared with the field measurements, one may conclude that the data generally approaches the data measured in the field.

Passband	Linear model	Correlation	F-test
Green	%=-12.7+0.99*DN	0.590	0.532
Red	%=-33.9+0.23*DN	0.629	0.653
NIR	%=-135.1+0.93*DN	0.997	152.77

(F_{critic} = 161.4 at 0.05 significance level)

Cultivate	Green band		Red band		NIR band	
	CS	S	CS	S	CS	S
Potatoes	6.1	7.5	5.7	8.3	60.7	64.2
Peas		6.7		5.7		54.0
Wheat	3.5	8.4	3.4	11.6	39.9	27.1
Sugarbeet	6.7	6.9	7.4	8.1	27.8	32.7
Grass	6.5	7.5	7.2	12.3	34.0	47.5
Bare soil	16.1	10.2	18.9	21.4	21.9	23.4

Cultivate	Green band		Red band		NIR band	
	CS	C	CS	C	CS	C
Potatoes	8.7	5.9	3.4	0.1	63.4	68.4
Peas		7.5		1.4		50.7
Wheat	4.6	3.4	2.4	0.2	44.9	47.0
Sugarbeet	8.3	11.5	6.4	9.3	29.0	34.2
Grass	8.8	8.3	5.6	4.0	36.7	50.5
Bare soil	16.7	15.1	20.1	15.1	22.7	29.3

Table 5 Reflectances of some cultivates, measured with the cropscan meter (CS), SILVACAM (S) and CAESAR (C) during the first test series. The SILVACAM values are bases on the given linear models.

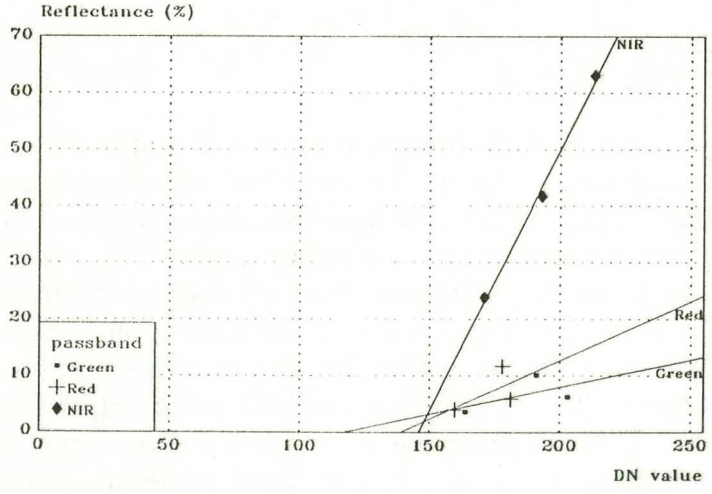

Figure 21 Video system response for the downward-looking mode based on three BCRS reflection panels. (Test1, July 1991).

4.8.1.2 Forward-looking mode

Also the video frames generated in the forward-looking mode were saturated. As the cropscan measurements are only valid for nadir calibration, the results obtained in the off-nadir mode will not be futher analysed.

4.8.2 Second test series

After revision of the Silvacam, the camera was tested indoors (see chapter 2) and outdoors. The outdoor tests were twofold: firstly some objects were recorded on the ground, secondly some agricultural fields in the Flevopolder were recorded from the air with the panels as reference targets. Only the downward-looking mode has been considered.

4.8.2.1 Ground test

Eight objects, among them 3 LMK panels (reflectances are given in table 3), were recorded on the ground with the Silvacam. The objects were recorded with a shutter speed of 1/1000 s, focal length 7 mm and iris stop f/9.5. With these settings the light fall-off will be negligible (paragraph 4.3). The white balance was set using the grey LMK panel as reference. In the second ground test series the preset white balance (colour temperature 5600 K) was used.

Passband	Linear model	Correlation	F-test
Green	%=-2.589+0.187*DN	0.990	41.35
Red	%=-1.962+0.301*DN	0.992	63.83
NIR	%= 0.081+0.324*DN	1.000	7017.46*

(F_{critic}=161.4 at 0.05 significance level; *significant model)

Object	Green band			Red band			NIR band		
	CS	Sg	Sp	CS	Sg	Sp	CS	Sg	Sp
Sand	25.2	29.7	27.6	33.3	37.2	33.8	44.9	48.6	45.5
Grass	5.2	10.6	6.4	6.9	7.1	5.7	31.5	35.6	35.8
Blue cloth	6.7	6.8	3.4	4.5	2.6	1.3	12.2	11.4	9.2
Green cloth	12.5	19.2	18.5	10.6	8.6	7.2	36.2	37.3	38.3
Red cloth	8.6	11.5	9.5	21.7	16.1	16.6	61.9	55.2	69.8

Table 6 Reflectances of some objects, measured with the cropscan meter (CS) and the SILVACAM. Sg: white balance set using grey LMK panel; Sp: preset 5600 K white balance. Linear relations are given in upper table.

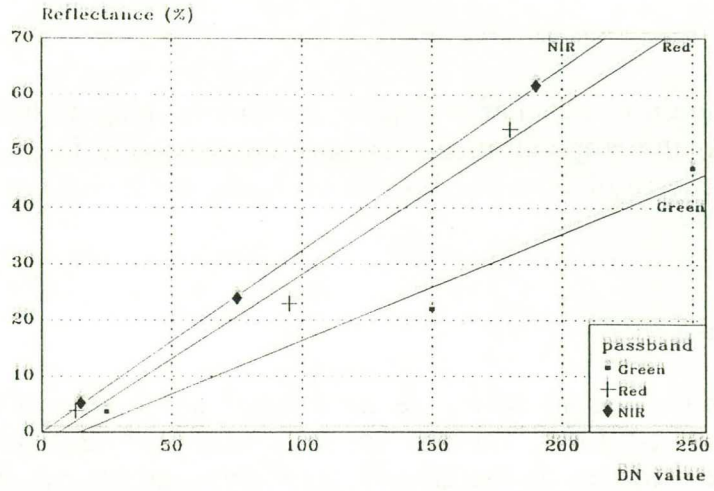

Figure 22.1 Video system response for the outdoor ground test based on three LMK reflection panels. (Test 2, June 1992).

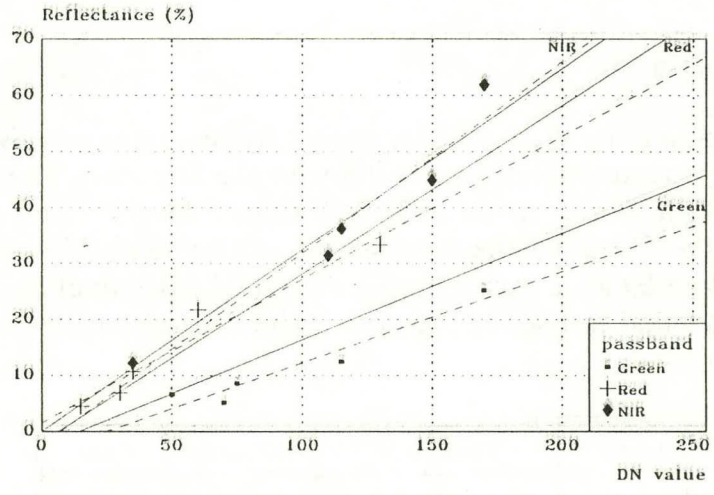

Figure 22.2 Object characteristics of sand, grass and cloths in relation to linear model based on LMK reflection panels, as shown in figure 22.1. The dashed lines are linear fits based on object responses.

Groundtruth has been collected with the cropscan meter (see chapter 3). These measurements were compared with the data generated by the Silvacam (table 6).

The first ground test yields well-defined linear models for all three passbands and a large dynamic DN-range (figures 22 and table 6). The linear model for the green passband shows a less steep slope indicating a higher susceptibility to the incoming radiant energy. This phenomenon is explained by the high spectral response of the CCD elements around 500 nm (figure 1).

Except for the NIR passband, all fits are to be rejected. The non-significant fit presumes a non-linear relation between DN values and reflectances. The bad fit of the linear models must be ascribed to a

shortage of points. Figure 22.2 shows the difference between the response based on the LMK panels and the other objects. The computed reflectances based on the models approximate the expected values very well (column Sg, table 6). When the preset white balance is used, the results improve for most objects (column Sp, table 6).

The results of the second ground test are much better then the results obtained during test 1. An appropriate white balance setting combined with a correct aperture appears to make the Silvacam an accurate radiometrical sensor, such that new airborne tests seemed to be justified.

4.8.2.2 Airborne test

On June 29th, 1992, tracks were flown over the Flevopolder using the revised Silvacam in a downward mode. Five LMK reference panels were positioned in the field. The same flight altitude of 1500 ft and 7 mm focal length were used as in July 1991 for comparable spatial resolution; shutter speed was 1/500 s and the aperture between f/5.6 and f/8. With the latter settings, light fall-off is negligible. During the flight, the video signal was stored on tape, using a JVC camcorder which was connected to the Silvacam. On the same day, reflectance characteristics of 12 agricultural fields were measured with the cropscan meter.

With the help of the reference panels, linear models were calculated for each of the three passbands (table 7). These models could not be based on all five panels for two different reasons:

- The dark grey LMK panel could not be discerned from the grass environment.
- The white panel generated saturated values in the green and NIR passbands.

Passband	Linear model	Correlation	F-test
Green	%=-23.5+0.250*DN	0.998	243.9*
Red	%=-11.7+0.271*DN	0.993	51.1
NIR	%=-24.3+0.292*DN	0.991	10.6

(F_{critic}=161.4 at 0.05 significance level; *significant model)

Table 7 Linear relations between reflectance and DN value based on LMK panels.

With these linear relations, the reflectance characteristics of 12 cultivates were calculated and compared with the cropscan meter measurements in the field. These values are shown in table 9, column P. Figures 23.1 through to 23.3 show the linear relations for both panels and cultivates.

Passband	Linear model	Correlation	F-test
Green	%=-12.7+0.161*DN	0.997	168.2*
Red	%=-5.1+0.180*DN	0.992	63.1
NIR	%=-28.9+0.498*DN	0.999	710.6*

(F_{critic} = 161.4 at 0.05 significance level; *significant model)

Table 8 Linear relations between reflectance and DN value based on three agricultural fields.

Cultivate	Green band			Red band			NIR band		
	CS	P	C	CS	P	C	CS	P	C
Grass	6.0	9.5	8.5	7.6	9.1	8.8	31.9	10.7	30.9
Wheat (high)	3.7	0.7	2.9	3.8	1.0	3.4	40.8	17.2	41.9
Wheat (low)	3.4	1.7	3.6	3.5	1.3	3.6	40.5	14.8	37.9
Peas	5.4	3.5	4.7	5.3	1.0	3.4	44.3	18.6	44.4
Potatoes	4.1	4.0	5.0	4.0	1.0	3.4	48.6	19.2	45.4
Sugar beet	5.2	5.0	5.6	5.1	2.9	4.7	51.0	20.4	47.3
Sugar beet*	4.9	3.5		4.9	2.6		43.1	17.7	
Potatoes	4.4	1.5	3.4	4.2	1.0	3.4	54.0	20.1	46.8
Beans*	11.3	13.7		14.1	17.8		18.3	3.1	
Wheat	3.6	0.2	2.6	3.8	1.8	3.9	39.6	17.2	41.9
Onions*	6.5	6.7		7.4	8.1		27.4	9.0	
Grass seed	5.2	6.2	6.4	5.7	5.9	6.6	47.7	19.5	45.8

*Cultivates used for linear model

Table 9 Reflectances of some cultivates, measured with the cropscan meter (CS) and the SILVACAM. Two different linear models are used, based on reflectance panels (P) and marked cultivates (C).

It appears that the computed crop reflectances are not too different from the expected ones in the green and red passbands. However, this might be misleading, as in these two passbands the range over which the linear model can be calculated is rather small. Deviations may occur, if higher values are considered. In the NIR passband, the linear model based on the panels does not agree with the registered DN values for the cultivates. The position of the linear fit generated by the panels in this particular passband is far above the line which would be generated when using agricultural fields as a reference. Therefore other linear models has been computed, based on three agricultural fields. Two of the tree linear relations are significant (see table 8). The reflectances, based on these models, are shown in table 9, column C. It appears that the computed values agree quite well with the cropscan measurements.

The ground tests, performed with the revised Silvacam in June 1992, make clear that the absolute radiometrical data, gathered by the video system, are reliable. However, once the system was airborne, the reference panels, generally used for aerial photography, did not comply for some reason.

Compared to other objects on the surface, too high reflectances were registered for these panels, particularly in the NIR passband. When

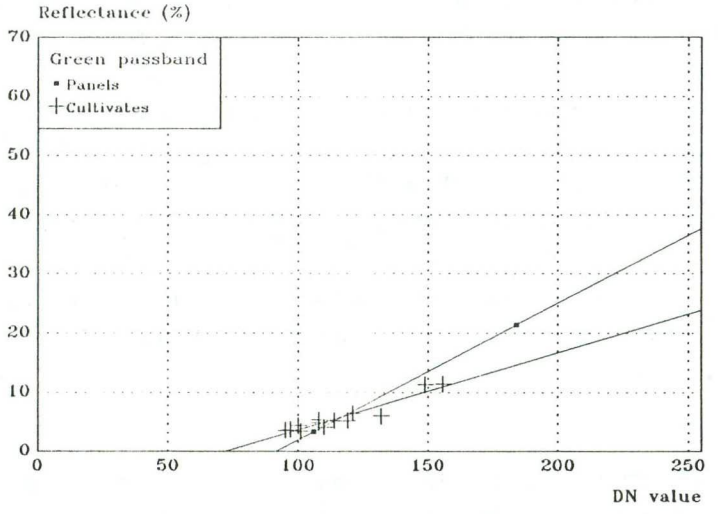

Figure 23.1 Video system response for vegetation and reflection panels. (Green passband).

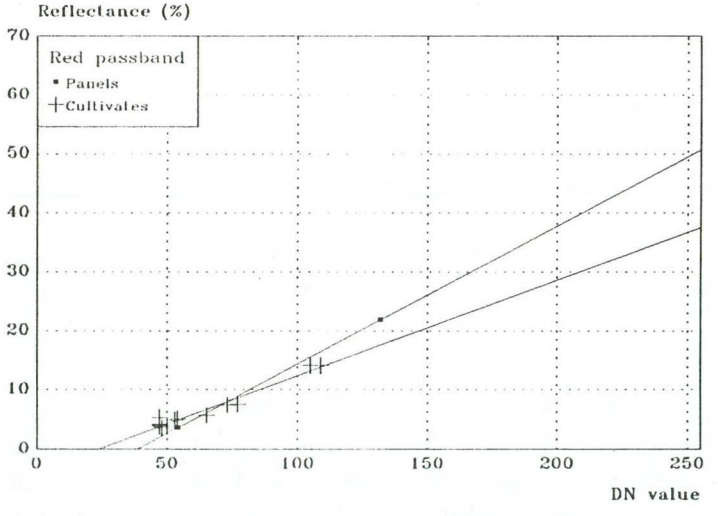

Figure 23.2 Video system response for vegetation and reflection panels. (Red passband).

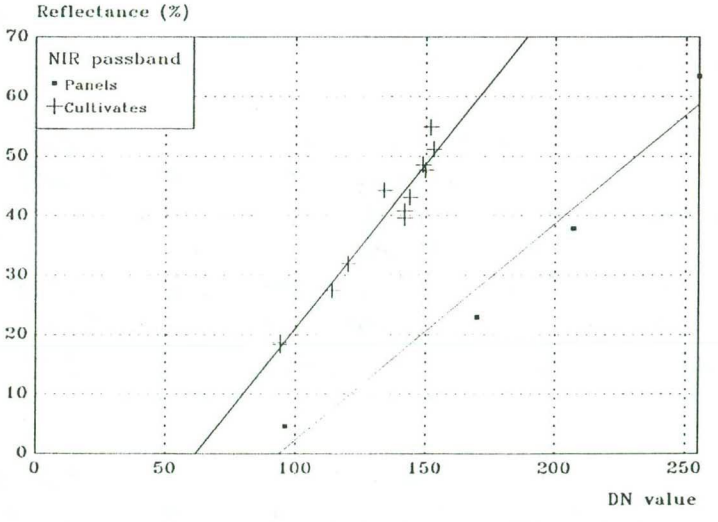

Figure 23.3 Video system response for vegetation and reflection panels. (NIR passband).

agricultural fields were used as a reference, the absolute radiometrical information gathered by the Silvacam proved to be reliable.

A reason for the registered low panel responses may possibly be that the panels are too small, in that the relating pixels get outshined by the grass background. As grass has a high reflectance in the NIR passband, this would result in especially the low-reflecting panels showing increased responses. Blur, resulting from the CCD elements being displaced in respect to the recorded object, would yield a similar effect. From figure 23.3 however, it appears that this is not the case, apart from the fact that the shutter speed as used in this test, is sufficiently short to prevent any blur.

Another reason might be that the panels do not behave as true Lambertian scatterers, or that the incoming light in the video camera is polarised. These phenomena would cause a lower amount of energy registered from these targets.

4.9 Classification

Having discussed absolute quantitative radiometrical information of objects, one may turn to image data being interpreted upon their relative numerical properties, regardless of their absolute radiometrical character. Here, it is identification and classification of pixels in video frames that counts.

In multispectral classification techniques, pixels with similar brightness values are grouped in several spectral classes. Identification of those classes corresponding to specific ground cover types, is carried out using appropriate classification techniques. Thus, raster images like video frames are converted to thematic ground cover images.

4.9.1 Schouwen area

On July 7th, 1991, a coastal dune area on Schouwen was recorded with the Silvacam from the air. The dune area is characterized by active blow-outs as well as stabilized dunes, and is being studied for several years by the Landscape and Environmental Research Group of the University of Amsterdam. Special attention is paid by this group to active blow-outs along the coastal zone, their size, shape and dynamics. The area is made up of a mosaic of contrasting ground features: very bright stretches of sand, surrounded by grass, shrubs and dark pine forests.

In a downward-looking mode several tracks were flown at an altitude of 5000 ft. The track was recorded with a shutter speed of 1/60 s and 7 mm

focal length. Several black, 4 x 4 m^2 georeference targets were positioned in the field at locations with known coordinates, in order to eventually correct the video frames for geometrical distortions.

As it turned out, the video frames appeared to be radiometrically saturated (plate 1), due to a combination of an improper white balance setting, a too large aperture and a long exposure time. The strongly contrasting ground coverage appeared to interfere with choosing appropiate camera settings.

The georeference targets could not be traced in the recorded frames, due to overexposure of the surrounding area. Especially the white sand in the blowout areas causes blooming, making the edges of these areas obscure. Blooming also affected the purity of the pixels over an extended area leading to a high amount of mixed pixels. The small dynamic range in all three passbands due to saturation - 50% of the pixels had DN values around 200 or higher - did not allow a good discrimination between different features on the ground.

4.9.2 Hulshorster Zand

In June 1992, with the revised Silvacam, a deflation area called Hulshorster Zand was recorded, an area which is similar to the recorded Schouwen area. This area consists of a mosaic of contrasting ground coverage. The same flight altitude was choosen in order to compare the results with the Schouwen area. The preset white balance was used (5600 K). The camera settings were: 7 mm focal length, shutter speed 1/500 s, iris f/8. Three black 4 x 4 m^2 targets were positioned on the white sands and one white 4 x 4 m^2 target was laid in a vegetated area to check blooming effects between the targets and the environment. The light conditions were comparable with those during the Schouwen flight.

From plate 2 it is clear, that the video recording has clearly improved. The vegetated areas show a lot of detail, as do the bright white sands. All four reference targets are distinctly discernable. Blooming effect of the white sand is negligible. A provisional thematic ground coverage map (plate 3) and a vegetation index image (plate 4) have been made on the basis of this image. The distinct vegetation classes in the ground cover map correspond to field observations. The results prove that the revised Silvacam is capable of discriminating between a diversity of different objects on their radiometrical characteristics.

CHAPTER 5

GEOMETRICAL PROPERTIES OF THE VIDEO CONFIGURATION

The foregoing chapter dealt with the radiometrical aspects of the Silvacam. Besides these aspects the camera might exhibit geometrical distortion caused by:

- Video camera optical system
- Relief displacement
- Variation of aircraft altitude
- Variation of aircraft velocity
- Aircraft drift

The geometrical accuracy and possible variations were tested indoors and outdoors. The indoor test has been performed under controlled conditions (light intensity, distance to illuminated object). The outdoor test took place above the city of Zeewolde, the Netherlands, which has a very regular geometrical structure.

Geometrical correction on grabbed video images has been done with the aid of program FATRAS (Braam et al., 1990). This program was developed at the Department of Surveying, Photogrammetry and Remote Sensing of Wageningen Agricultural University and is used to perform geometrical transformation on raster images and match such images with topographical tie points. FATRAS is based on the matching of Delaunay triangles (McCullagh & Ross, 1980). The tie points were adjudged to the video images with the aid of program ILWIS, an image processing package developed by the International Institute for Aerospace Survey and Earth Sciences (ITC), Enschede, The Netherlands.

5.1 Geometrical distortion measurement

A method of measuring the geometrical deformation of a raster image is to transform the image to a raster image with known control points. The transformation program FATRAS matches a raster image to a geometrical reference system (metrical or geographic coordinate systems): ground control points (GCPs) from the original image (the *slave*) have to match points with known coordinates in a reference system (the *master*).

The Delaunay procedure involves constructing triangles from the control points. The procedure results in two sets of triangles: one for the master and one for the slave. Using the pairs of master/slave Delaunay triangles, an affine transformation parameter set is calculated for each pair making

the slave facet matches the corresponding master facet. Only the pixels inside that specific triangle are transformed according to those parameters. Pixels which are not enclosed by a facet will be excluded from the transformation and are left out from the resulting image. FATRAS resamples the pixels according to the *nearest neighbour* methodology.

As FATRAS generates local transformation parameters, these parameters can be compared with each other to test geometrical deformation within an image. This makes FATRAS very useful for the detection of local deformation caused by the camera system. Two tests are performed:

- Triangle test
- Second neighbour test

5.1.1 The triangle test

In an affine transformation, two transformation parameters are defined:

- The *rotation* of a facet along X- and Y-axis (α_x and α_y, respectively).
- The *scaling* (stretching or shrinking) of a facet along X- and Y-axis (S_x and S_y).

If α_x and α_y differ, an angle deformation will result and a rectangular grid will become an oblique one. If S_x and S_y differ, a deformation in the distance result. The parameters tested are angle distortion δ and scale distortion R:

$$\delta = \alpha_x - \alpha_y$$
$$R = S_x / S_y$$

If a whole raster image is affinely deformed, the parameters δ and R will be the same for all triangles. Local deformations in the image will result in different parameters for each facet.

5.1.2 The second neighbour test

The second neighbour test is used to detect errors in the appointment of GCPs. This is done by predicting the position of a GCP with respect to neighbouring triangles within a user defined radius. Based on the affine transformation parameters the position of the GCP is calculated. The difference between the predicted and the calculated position of a GCP is called the predicted rest vector. This vector is indicative for the accuracy of GCP appointment.

5.2 Indoor test

A millimetre grid was recorded indoors with the conventional CCD video camera at three different focal lengths: 30, 50 and 97.5 mm. A millimetre grid offers a high amount of ground control points (GCPs) which can be measured with high accuracy and are equally spread over the video image. Video frames were grabbed in a standard mode of the video board (512(h) x 576(v), pixel depth 32 bits). This mode does not yield square pixels but rectangular pixels with h:v = 1:≈0.669. The resulting raster files were split to three separate colour planes. Only one of these files was tested on local geometrical deformation as it is assumed that geometrical distortion is independent of the passband. GCPs were appointed by means of ILWIS, slave GCPs are expressed in (row,column)-coordinates whereas the master GCPs were given in metrical coordinates by the interpreter. These data were presented to FATRAS for further analysis.

Figures 24 to 26 show the geometrical distortions δ and R and the rest vector values for a millimetre grid recorded with three different focal lengths: 30, 50 and 97.5 mm, respectively. The results are given in table 10.

		f=30 mm	f=50 mm	f=97.5 mm
Distance camera-object (cm)		164.5	164.5	94
Area size (mm) Resolution (mm/pixel)		311(h)x240(v) 0.63(h)x0.42(v)	189(h)x148(v) 0.38(h)x0.26(v)	91.5(h)x71.5(v) 0.19(h)x0.12(v)
Number of control points Number of triangles		97 158	82 130	56 84
R	Mean St.dev.	0.671 0.009	0.671 0.007	0.669 0.007
δ (rad,°)	Mean St.dev. Maximum	0.028 (1.6°) 0.016 (0.9°) 0.06 (3.5°)	0.028 (1.6°) 0.012 (0.7°) 0.05 (2.9°)	0.026 (1.5°) 0.011 (0.6°) 0.05 (3.0°)
Rest vector (pixels)	Mean St.dev. Maximum Maximum (mm)	1.142 0.230 1.8 1.11(h)x0.74(v)	1.028 0.255 2.3 0.88(h)x0.60(v)	1.194 0.250 2.0 0.38(h)x0.24(v)

Table 10 Geometrical deformation parameters for three focal lengths.

The distortion parameters generated by FATRAS reveal local distortion if present. The distortion in the frames might be considered negligible if one takes into account that errors may occur during the GCP-appointment due to small inaccuracies. The indoor tests show no preferable location of the distortion parameters in the video frame.

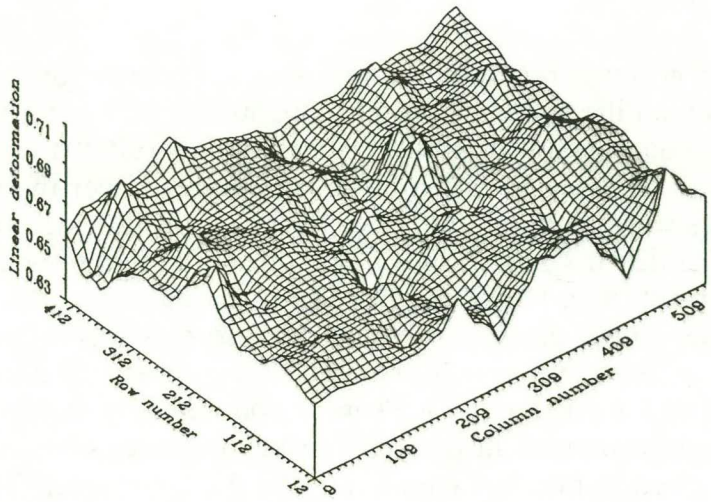

Figure 24.1 Spatial distribution of scale deformation parameter R for f = 30 mm.

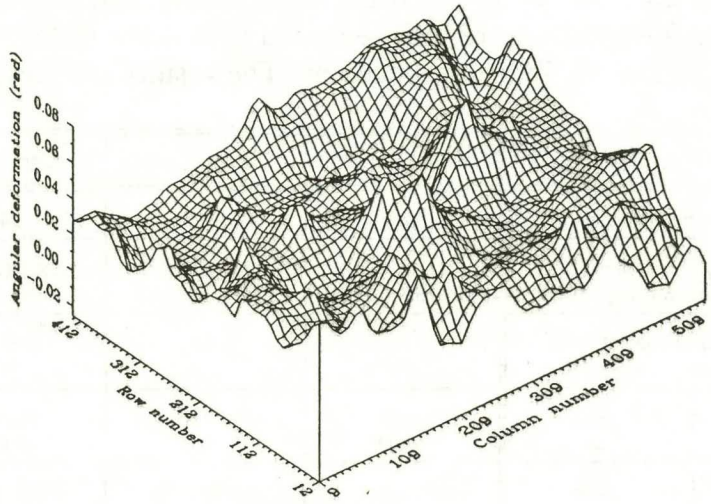

Figure 24.2 Spatial distribution of angle deformation parameter δ for f = 30 mm.

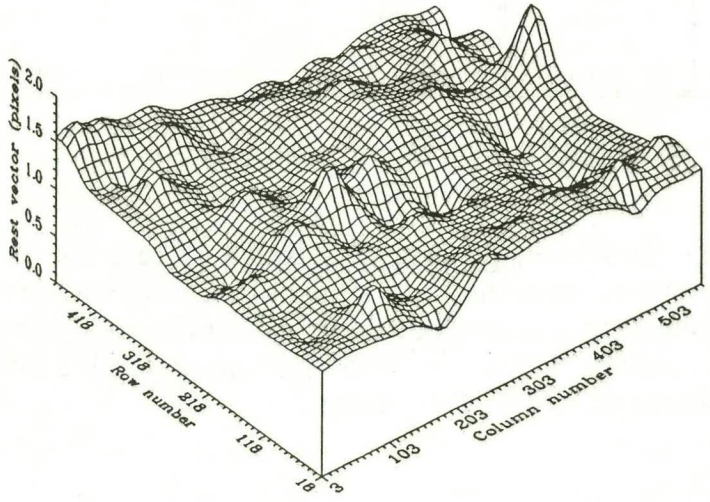

Figure 24.3 Spatial distribution of the mean rest vector for f = 30 mm.

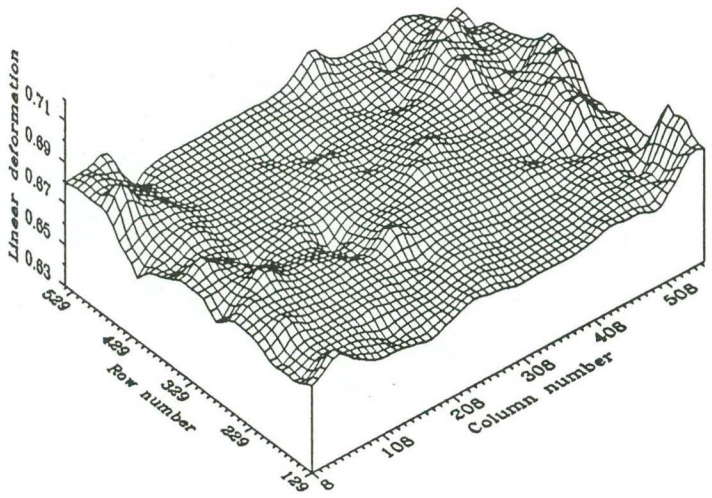

Figure 25.1 Spatial distribution of scale deformation parameter R for f = 50 mm.

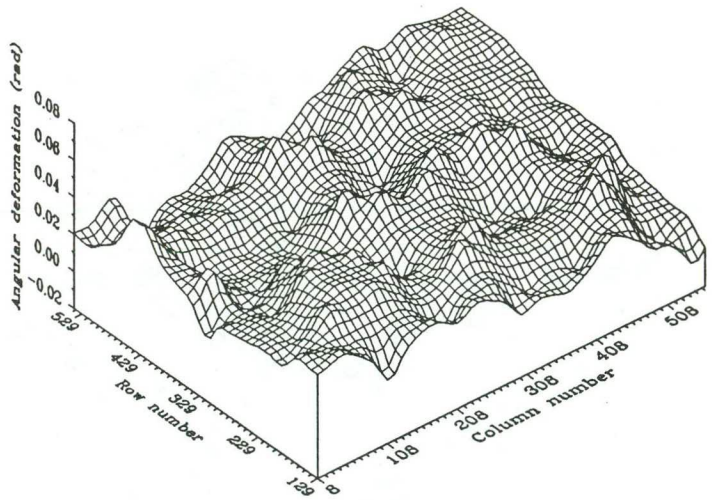

Figure 25.2 Spatial distribution of angle deformation parameter δ for f = 50 mm.

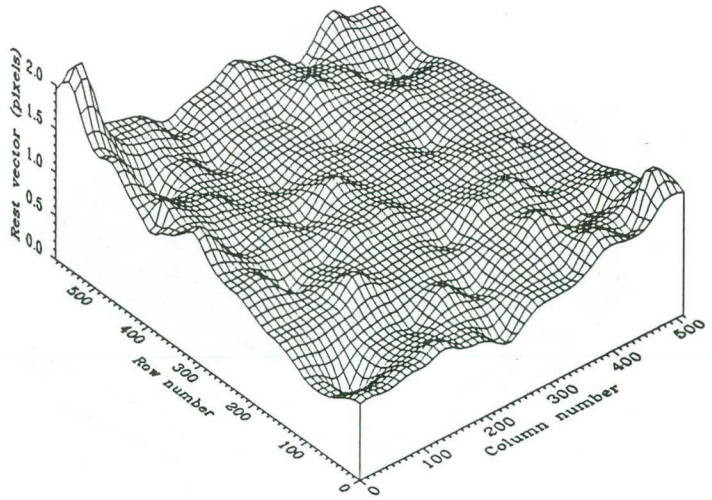

Figure 25.3 Spatial distribution of mean rest vector for f = 50 mm.

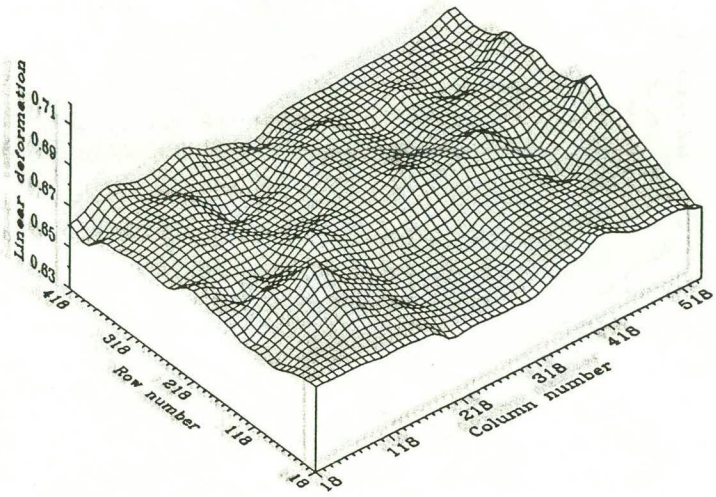

Figure 26.1 Spatial distribution of scale deformation parameter R for f = 97.5 mm.

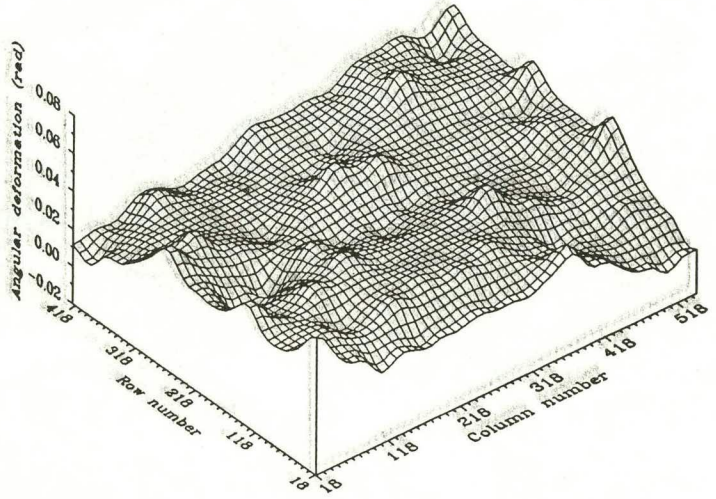

Figure 26.2 Spatial distribution of angle deformation parameter δ for f = 97.5 mm.

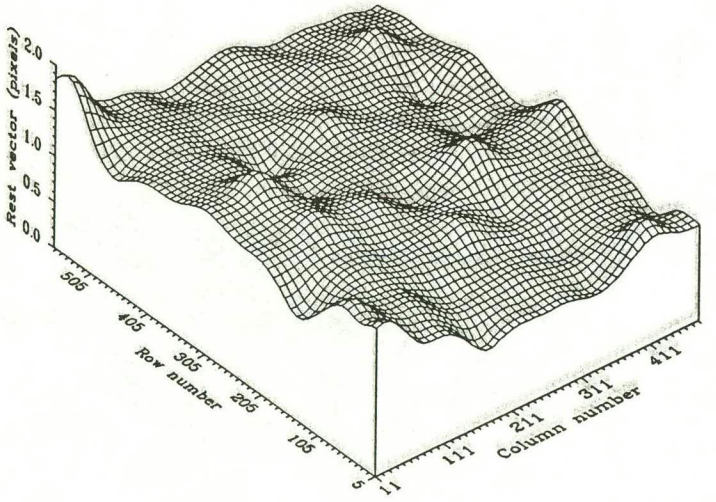

Figure 26.3 Spatial distribution of mean rest vector for f = 97.5 mm.

5.3 Outdoor test

The indoor results reveal no significant geometrical distortion for the CCD video camera. However, practice shows that geometrical accuracy not only depends on the sensor but also on the appointment of the GCP set of the slave (video frame) as well as for the master. The latter is usually obtained by reading a topographical map with a digitizer. Such maps may include scale dependent errors. To test the spatial accuracy of a video frame, a track was flown above Zeewolde.

A 1:10,000 topographic map of Zeewolde on scale-fixed material was used to read the master coordinates with a digitizer. The maximum appointment accuracy of the digitizer (a Calcomp 9100) is about 0.1 mm. The appointment accuracy error for the master GCP is therefore approximately 1 m.

The flying altitude of 1500 ft and a focal length of 7 mm yields a ground resolution of 0.76(h) x 0.74(v) m/pixel for the video frame. The slave and master coordinates were interactively obtained by the program ILWIS. To illustrate the overall appointment accuracy of the coordinates in both systems (master and slave), the affine transformation system of ILWIS revealed a ground resolution of 0.767 m/pixel and a standard deviation of 1.24 pixels for the entire frame when the set of 20 slave GCPs were transformed. We are interested, however, in the local distortion parameters. Therefore program FATRAS has been used. The results are shown in figures 27.1 to 27.3, and table 11 shows the values.

Area size (m) Resolution (mm/pixel)		510(h)x380(v) 0.76(h)x0.74(v)
Number of control points Number of triangles		20 28
R	Mean St.dev.	0.693 0.016
δ (rad,°)	Mean St.dev. Maximum	-0.174 (-10°) 0.020 (1.1°) 0.06 (3.5°)
Rest vector (pixels)	Mean St.dev. Maximum Maximum (m)	3.595 0.776 5.3 4.02(h)x3.97(v)

Table 11 Geometrical deformation parameters for Zeewolde area.

The mean scale deformation parameter of all triangles is 0.693, which approximates very well the expected value of 0.669. The largest scale distortions are found in the upper left part of the frame. The centre of the

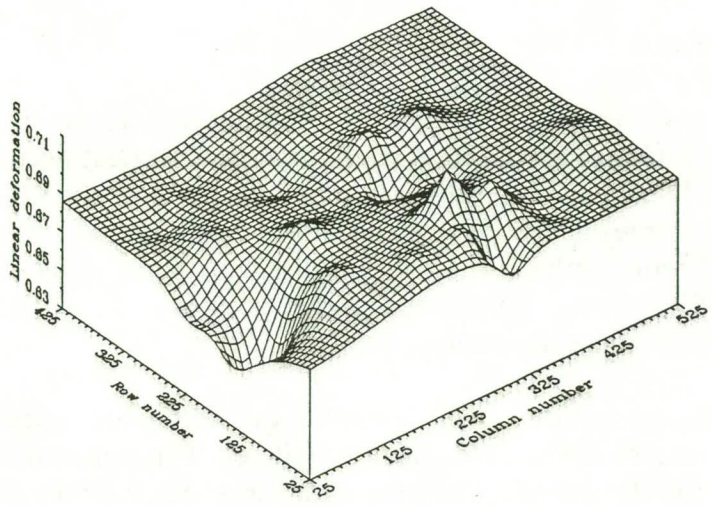

Figure 27.1 Spatial distribution of scale deformation parameter R for Zeewolde.

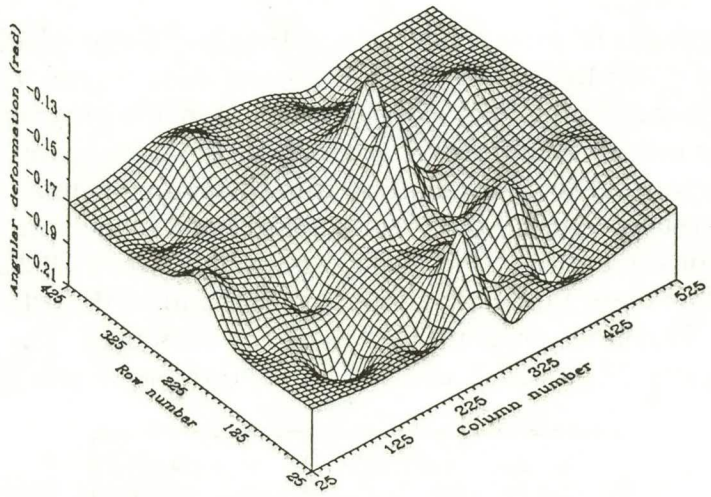

Figure 27.2 Spatial distribution of angle deformation parameter δ for Zeewolde.

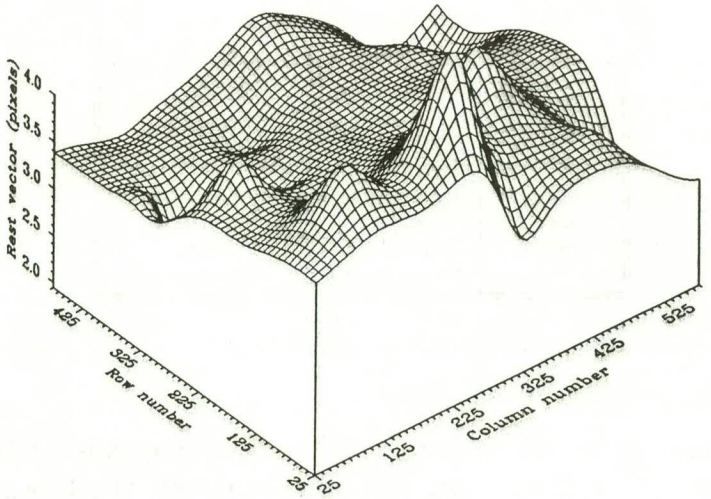

Figure 27.3 Spatial distribution of mean rest vector for Zeewolde.

video frame shows the smallest angular distortion. The rest vectors of the GCPs are especially high in the upper half of the video frame.

With this GCP set the slave image was transformed with the master coordinates. The original video image is shown in plate 5, together with the Delauny facets. The transformed image is depicted in plate 6. Pixels which were not enclosed by a facet, have been excluded from the geometrical transformation and are not shown in plate 6.

The outdoor geometrical test results show less accurate values than the indoor tests. Besides inaccuracies in the map, these results can also be explained by a combination of the non-equilateral shape of facets and the appointment inaccuracy of certain GCPs. The relatively high but unanimous deformation from the orthogonal projection (δ) must be explained by yaw-distortion during flight caused by wind.

With the used flying altitude and camera settings the overall inaccuracy of a point in the video frame is about 2 to 2.5 m. It depends on the features to be studied if this resolution is acceptable for the interpreter to detect or monitor changes within the ground surface pattern. If not, the camera settings and/or the flying altitude should be altered until an acceptable ground resolution is achieved.

CHAPTER 6

OPERATIONALIZATION OF VIDEOGRAPHY

6.1 Feasibilities

Now that radiometric and geometric properties of the video configuration have been tested thoroughly, the next thing to do is to look at actually operating the system. There are several ways of operating, and the choice which way to choose depends largely on what the end user wants for a result from a particular operation.

The most simple and also the easiest way to use a video camera is to real time look at the video screen and analyse the images instantaneously. The video tape in that case is supposed to be a kind of back-up for one's own memory. One may rightly throw in that looking at the real world is more affective. However, it may as well be an advantage to have an analogue tape on which to rely in case of doubt.

The next step in operating a video system is in grabbing, i.e. digitizing images from the tape, once the flight is over. Depending on the user's needs, one may select images, either hand-pick them, or grab them automatically. These are raw material, to be visually analysed on the video screen.

Grabbing an image opens up a host of feasibilities, in that the digitized image, consisting as it does, out of three separate bands, can be processed in many ways, including e.g. classifications, vegetation indexing, density slicing, calibration, geo-correction. The latter two may serve as preparations for a procedure called mosaicking, i.e. combining an indefinite number of images into a single large image. A mosaick may be formed out of a 1-dimensional series of original images, a ribbon, or out of a 2-dimensional network of images, covering a whole area. Mosaicking however, is not part of the present project.

The array of feasibilities that is opened up by grabbing images, may well result in nicely problem-tailored processing activities. For every user, every problem and every single project, large or small, each according to its character, one will decide as to what sort of processing to choose. Again, presentation of the results, usually as hardcopies, is still another matter.

Geocoding of the images comes in at an early stage of the operation. The most simple way is by using detailed maps as a source of reference. Such maps may not be available however, the areas to be surveyed may lack the necessary detail or they may be very extensive, resulting in surveys being

rather complicated. This is when a Global Positioning System (GPS) is of great use in bringing structure in the whole operation, as well as pinpointing each and every single video image to the real world. Ideally the GPS signals are being superimposed on the video tape, for geocoding to be carried out in the laboratory. GPS is outside the scope of the present project.

Videography clearly is a fast earth observation technique. It depends on the character of the area involved, on the problem to be solved and on the user who is to work on the basis of the results, how to implement the technique in e.g. a research or monitoring programme.

6.2 Pricewise

Videography is a fast earth observation technique, it is an inexpensive one too. What does that mean? Small, cheap aircraft can be used as a platform. The system's hardware and software amount to something between US$ 50.= and US$ 100.= for most purposes, according to the user's needs. Video tapes are easily to come by and fairly inexpensive. Moreover, they can be used again if so wished. But this does not yet indicate a precise price for videography.

A comparison of some sorts with costs of aerial photography might be worthwhile to try. For the purpose, assumptions would have to be made, e.g. regarding the extention of the area, the scale of the photo's and the pixel size of the video images. For an area of, say 100 km^2, prices for CIR aerial photography hard copies may be said to range from US$ 50.= to US$ 500.= per km^2 approximately, for PSR's (photo scale reciprocals) ranging from 40,000 to 2,500.

In videography, the raw material should not be considered to be hard copies, but rather digitized frames, ready for image processing to be carried out. Their cost will not nearly be a quarter of the price of aerial photo's.

6.3 Map making

From the above paragraphs is may be clear that videography is a fast and relatively inexpensive earth observation technique in its own right, as well as to be used as an extra means for calibration or classification (cf. ground truth finding) of e.g. satellite images. Being a simple earth observation tool, it can be brought into operation virtually all over the world, for many different applications, especially when large scale observation is required or when ribbon-like structures like roads, rivers or coastlines are to be monitored, or when - in event-based surveys - quick assessments have to

be made. Other applicational fields are e.g. forestry, crop cultivation, irrigation, mining, water quality control, environmental management, etcetera, including vegetation index-, or leaf area index-based analyses. Finally, map making can be carried out using GPS, and mosaicking of the video frames.

CHAPTER 7

CONCLUSIONS AND RECOMMENDATIONS

The first test series in July 1991 revealed a considerable matter in dispute, relating to the white balance procedure, which is ment to supply a correct balance between the three video channels under changing light conditions. The balance has to be set in order to correct for colour temperature. The procedure is standard carried out while holding a white object in front of the lens. As an alternative for the CIR camera, the same procedure was carried out while flying above an unspecified vegetated area. Neither lead to satisfactory results. In the latter case, an insusceptible red video channel (NIR passband) and a distorted mutual balance between the three video channels were the result. As a consequence, the sensibility for the incoming radiant energy became passband-dependent which, in combination with a large aperture and/or a long shutter speed, resulted in saturated video images, a small dynamic range and therefore unreliable reflectance values, as compared to values measured with the cropscan meter.

The coastal dune area at Schouwen was recorded with the Silvacam, on the basis of the above alternative balance prcedure (see plate 1). The saturated video raster images are characterized by a very small dynamic range - 50% of the image pixel values were above DN value 200, rendering the discrimination between spectral classes difficult.

A second test series was performed indoors as well as outdoors in June 1992, using the revised Silvacam. A new feature of the camera was the preset white balance, related to a colour temperature of 5600 K ("noon daylight"). Both manual settings and preset white balance were successfully used. The relation between the video signal and the DN values of the digitized images could be satisfactorily described by a linear relation (figures 4 through to 6). Two points should be made:

- The CCD elements are relatively sensitive around 500 nm. As a consequence, the blue video channel (green passband) of the Silvacam is more susceptible to the incoming radiant energy than the other channels. This does not influence the radiometrical accuracy of the Silvacam. The phenomenon however is not properly corrected for.

- In the NIR passband, uniformly reflecting, screen filling objects generate higher DN values in the centre of the screen compared to the periphery, probably due to reflection of NIR radiation in the lens system. Differences may be in the order of 10% and disappear when larger

apertures are set. A different type of lens coating may solve the problem.

The right camera settings for specific light conditions, e.g. shutter speed and diaphragm, possibly the use of neutral density filters, will yield good video images. A change in one of these camera settings, according to our test results, will influence the incoming radiant energy in a non-linear way (figures 13 through to 15). These non-linear changes may be of no interest when objects within one frame are analysed and classified according to their multiband spectral characteristics. If one is interested in the absolute reflectance characteristics of objects however, camera settings should be unaltered during flight. In highly contrastating environments, the best way to obtain a well-defined dynamic range for all three passbands without under-or oversaturation, is to record the scene more than once with different settings or by using ND-filters. The latter however disperse the incoming light thus influencing the image quality in an uncontroled way.

The Silvacam has no correcting mechanism for the radial decrease of incoming light caused by the interaction between the lens system and the CCD facetplate. This feature (light fall-off) was shown to yield decrease of upto 60% towards the periphery of a frame when a large aperture was combined with a large focal length. Even so, an aperture of f/5.6 or smaller showed a radial decrease in the order of 10% or less. Depending on the required radiometrical accuracy, one may decide to correct for this feature as yet.

The read-out of tape-stored analogue video signals is influenced by the storage medium and by the VCR. The said signals yield higher DN values then non-tape stored signals. As a consequence, effects of saturation are accomplished faster if the signal is stored on tape. The use of different types of VCR does not influence the overall DN value of a frame. Even so, the variance of DN values is larger when qualitative low-performing recorders are used.

Remarkably, there is quite a difference between reference panel responses as registered on airborne video images, and absolute radiometrical characteristics of the same. The first DN values appeared to be too high, compared to those of the cultivates. This holds particularly for the NIR passband. The radiometrical distortion only occurs when the video system is airborne. This may possibly be caused by the size of the panels in respect to the spatial resolution, with blooming of the reference panels as a result.

The reflectances of the vegetated fields as registered on airborne images however, do match with those measured by the cropscan meter, thus bringing operational radiometrical processing of video images in the bounds of possibility (see plates 3 and 4).

For the purpose of geometrical validation of the video images, two local deformation parameters were tested: angle and scale deformation. The parameter values appeared to be similar allover the video frame. Indeed, they may be considered to be negligible for most purposes, for the used lens system. The main inaccuracies were caused by the mutual positions of the ground control points and the digitizing thereof in the test procedure.

The results of the present project may be considered to be a sound basis for further developing CIR CCD-video remote sensing into a commercially workable technique. The latter matching Cartoscan's objectives in the field, the company aims at developing the right video system for the purpose.

REFERENCES

BRAAM, B.M., H.J. BUITEN, D.H. HOEKMAN, AND H.J.C. VAN LEEUWEN (1989),
Analyse van VARAN-S en IRIS radarbeelden, geautomatiseerde geometrische verwerking en data extractie.
BCRS report #89-37, 135 pp.

CLEVERS, J.G.P.W. (1986),
Application of Remote Sensing to agricultural field trials.
Agricultural University Wageningen Papers 86-4, 227 pp.

DONZE, M. ET AL. (1989),
CAESAR: performance and first evaluation of application possibilities.
BCRS report #89-06, 101 pp.

ELEVELD, M.A. (1992),
The usage of video images in research of geomorphological processes in the coastal dunes of Schouwn.
Internal report of the Landscape and Environmental Research Group, Amsterdam University, 25 pp.

EVERITT, J. AND P. NIXON (1985),
False colour video imagery: a potential remote sensing tool for range management.
Photogramm. Eng. and Remote Sensing (51)6, pp. 675-679.

HUTCHINSON, C.F., R.A. SCHOWENGERDT AND R.L. BAKER (1990),
A two-channel multiplex video remote sensing system.
Photogrammetric Engineering and Remote Sensing (56)8, pp. 1125-1128.

KING, D., D. JAYASINGHE AND J. VLCEK (1986),
Spectral and spatial analysis of multiband video images.
Proc. 52nd meeting ASPRS, Washington D.C., pp. 85-91.

KING, D. AND J. VLCEK (1990),
Development of a multispectral video system and its application in forestry.
Can. Journ. Remote Sensing (16)1, pp. 15-22.

LIMANN, O. AND H. PELKA (1991),
Televisietechniek.
Kluwer Technische Boeken bv Deventer, 456 pp.

MCCULLAGH, M.J. AND C.G. ROSS (1980),
Delaunay triangulation of a random data set for isarithmic mapping.
Cartographic Journ. 17, pp. 93-99.

MOZER, M. AND P. SEIGE (1971),
High resolution multispectral TV camera system.
Proc. 7th Int. Symp. on Remote Sensing of Env., Ann Arbor, Michigan, pp. 1475-1480.

ROBINOVE, C. AND H. SKIBITZKE (1967),
An airborne multispectral video system.
U.S. Geol. Survey Prof. Paper 575-D, pp. D143-146.

SHAW, G. AND WHEELER, D. (1985),
Statistical techniques in geographical analysis.
John Wiley & Sons, 364 pp.

SLATER, P.N. (1980),
Remote Sensing Optics and Optical Systems.
Addison-Wesley Publishing Company, 575 pp.

SMORENBURG, C. AND A.L.G. VAN VALKENBURG (1986),
Radiometrische calibratie van de CAESAR scanner.
TPD TNO-TH report, Delft.

VLCEK, J. (1983),
Videography: some remote sensing applications.
Proc. 50th meeting ASPRS, Washington D.C., pp. 63-69.

VLCEK, J. AND D. KING (1985),
Development and use of a 4-camera video system in resource surveys.
Proc. 19th Int. Symp. on Remote Sensing of Env., Ann Arbor, Michigan, pp. 483-489.

YUAN, X., D. KING, J. VLCEK AND D. MCLAUGHLIN (1989),
Application of aerial multispectral videography and colour/colour IR photography in sugar maple decline assessment.
Proc. 12th Can. Symp. on Remote Sensing, Vancouver B.C., pp. 2385-2389.

GLOSSARY

A/D	Analog to Digital
C	Chrominance (colour hue and saturation)
CCD	Charge-Coupled Device
CCIR	Comité Consultativ International des Radiocommunications
CIR	Colour infra-red
Composite video	Total video signal including luminance, chrominance and synchronisation
FATRAS	Facet Transformation
ILWIS	Integrated Land and Water Information System
NTSC	National Television System Committee
PAL	Phase Alternating Line
RGB	Red-Green-Blue
SECAM	Systeme Couleur avec Memoire
S-VHS	Super-VHS
VHS	Video Home System
Y	Luminance (brightness)

PLATES

COLOUR INFRARED VIDEO IMAGE

SCHOUWEN (June 1991)
Blowout dune system
natural reservoir "De Eendenkooi",
Schouwen, The Netherlands.

Frame size: 1.4 x 1.0 km^2
Spatial resolution: 2 x 2 m^2
Flying altitude: 5000 ft

Camera settings:
Iris: f/8
Shutter: 1/1000 s
Focal length: 7 mm

CARTOSCAN

Plate 1 Colour infra-red video image of the coastal dune area of Schouwen, recorded with the SILVACAM on July 9th, 1991. The white balance was set on an unspecified area during flight.

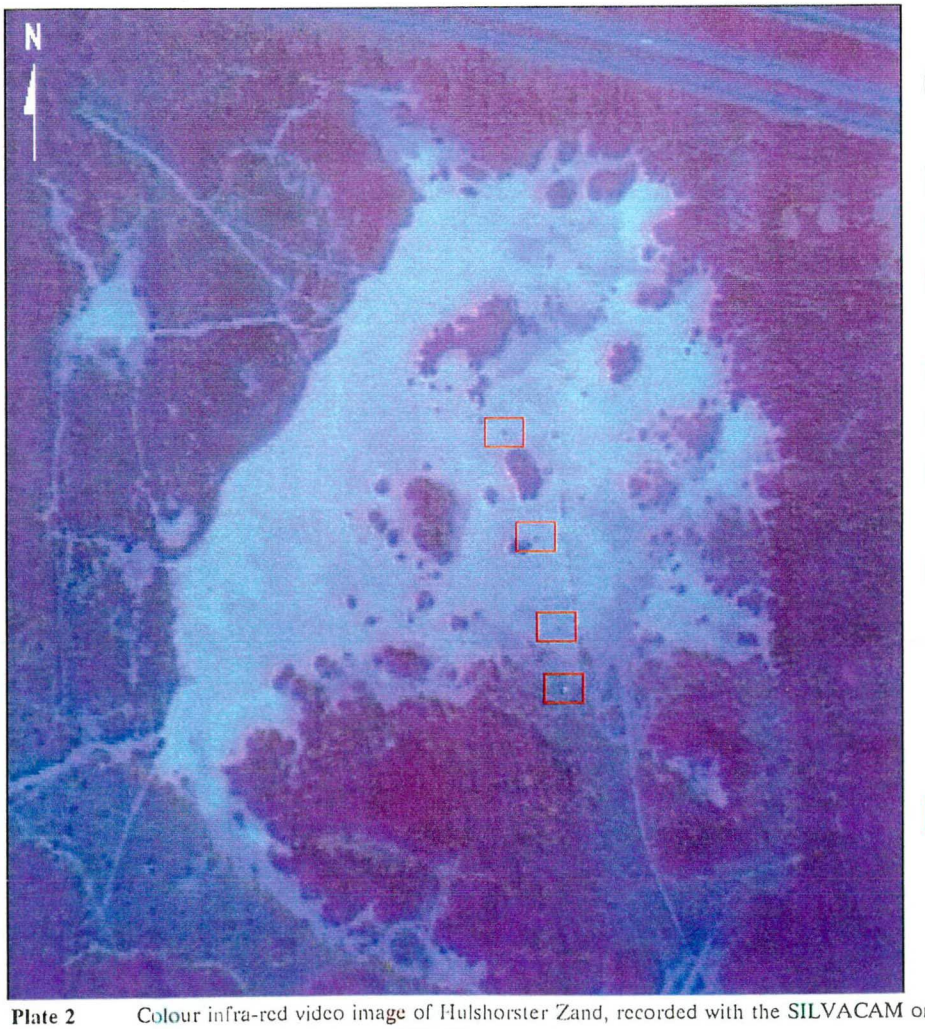

COLOUR INFRARED VIDEO IMAGE

HULSHORSTER ZAND (June 1992)
Deflation area near Harderwijk,
the Netherlands.

Frame size: 1.4 x 1.0 km^2
Spatial resolution: 2 x 2 m^2
Flight altitude: 5000 ft

Camera settings:
iris: f/8
shutter: 1/500 s
focal length: 7 mm

Position of targets (4 x 4 m^2) for georeference

CARTOSCAN

Plate 2 Colour infra-red video image of Hulshorster Zand, recorded with the SILVACAM on June 29th, 1992. Preset white balance (5600 K) was used.

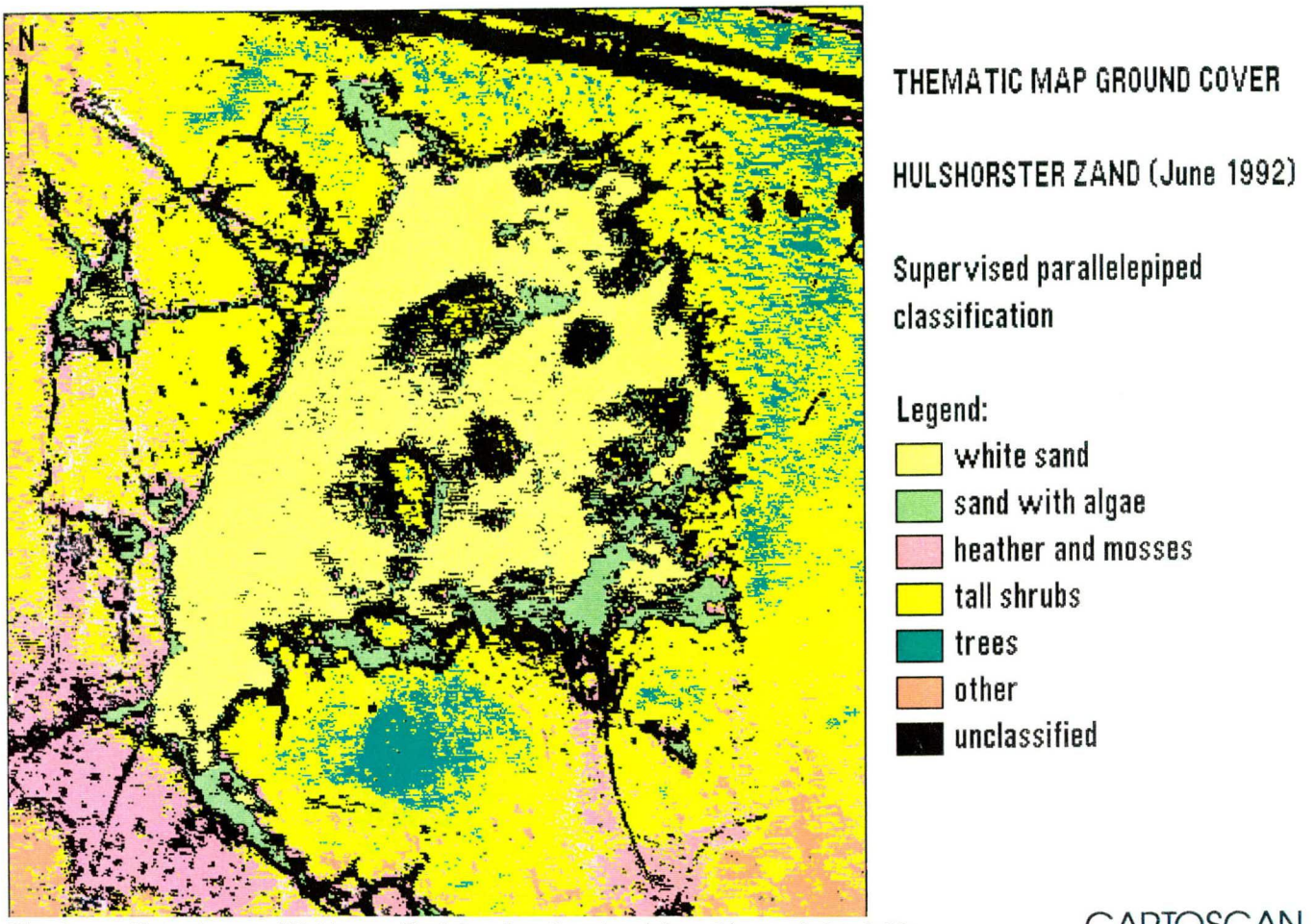

Plate 3 Thematic map of Hulshorster Zand, based on the colour infra-red image of plate 2. The parallelepiped classification method is used for six classes and an a-priori knowledge of the ground coverage (supervised classification).

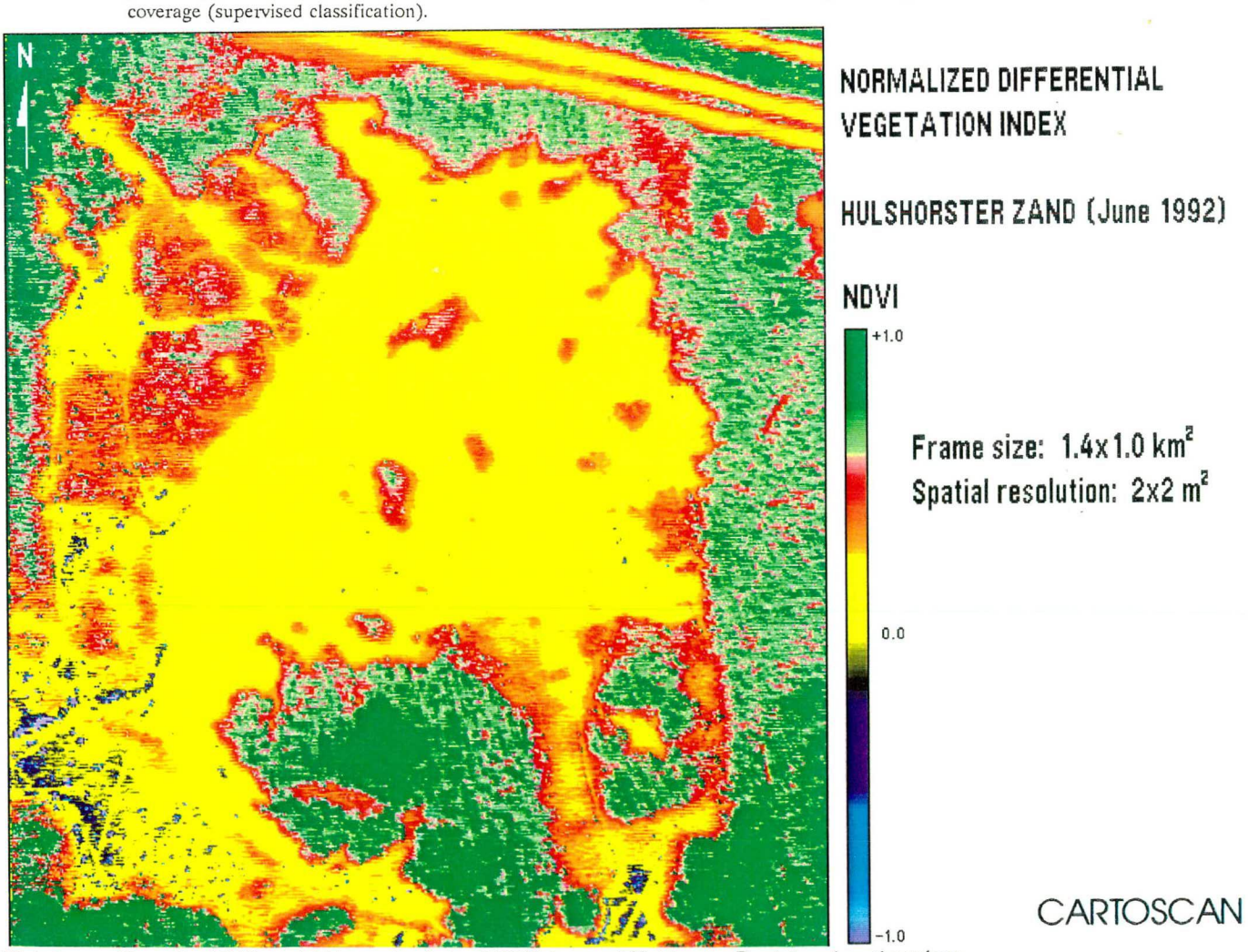

Plate 4 Normalized Differential Vegetation Index (NDVI) image of Hulshorster Zand, based on the colour infra-red image of plate 2. The NDVI is the difference between the infra-red and the red passbands, scaled between -1 and +1, and is a criterion for the amount of active chlorophyll.

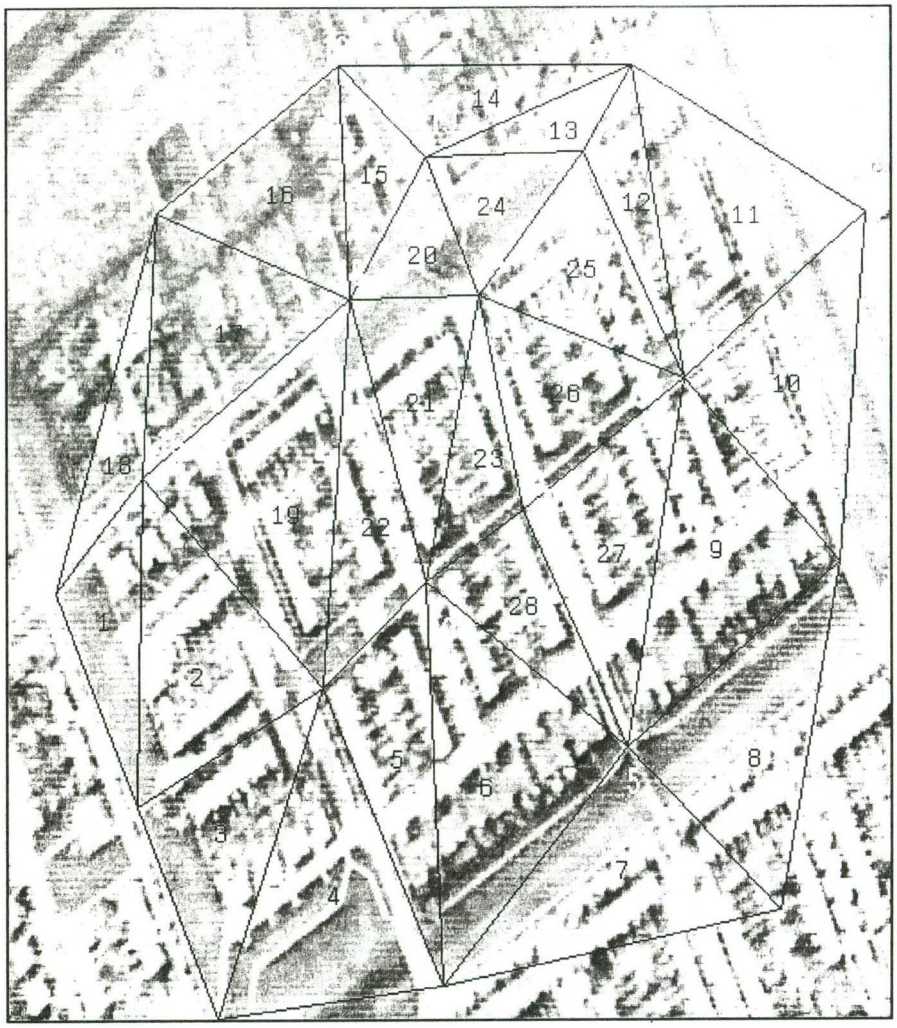

COLOUR INFRARED VIDEO IMAGE

ZEEWOLDE
Overlay of slave facets upon a video frame of Zeewolde village, The Netherlands.

20 GCP's
28 triangles

Triangle deformation parameters:
R = 0.693
δ = 0.174 rad

CARTOSCAN

Plate 5 Colour infra-red video image of Zeewolde village. Altitude is 1800 ft, focal length 7 mm, shutter 1/500 s. Total video frame is 510 x 380 m^2, spatial resolution 0.76 x 0.74 m^2. The overlay (red) represents the Delauny facets based on the slave coordinates.

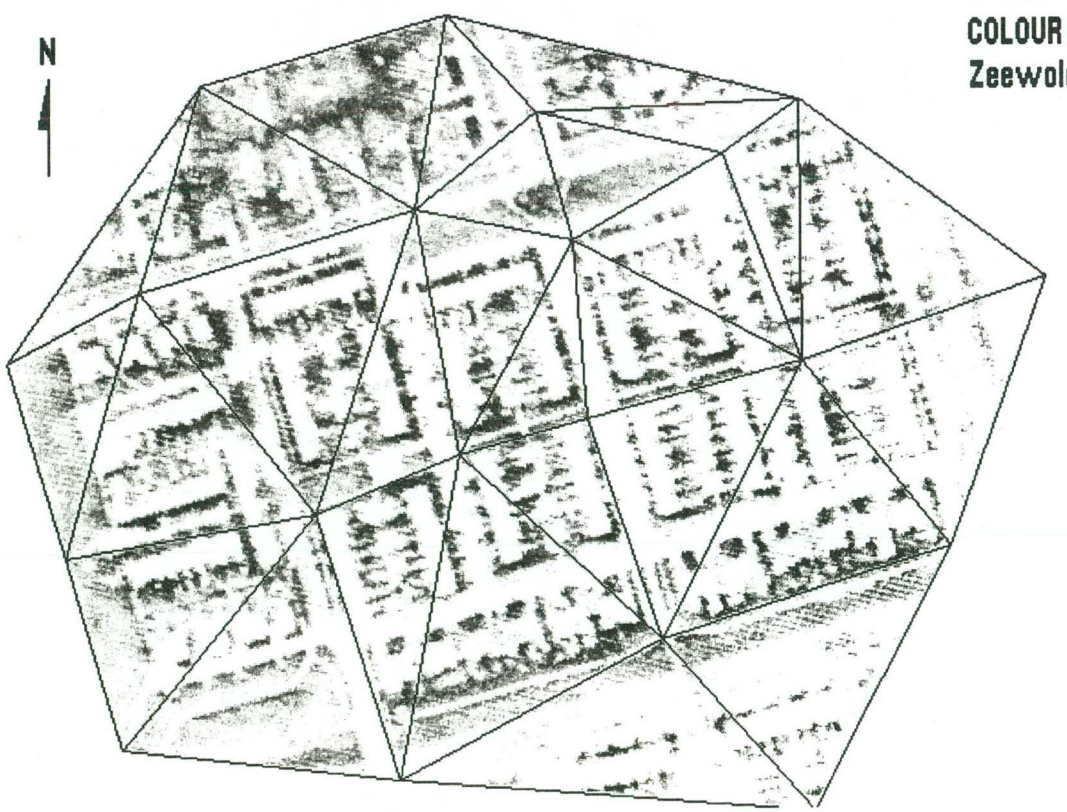

GEOMETRIC TRANSFORMED COLOUR INFRARED VIDEO IMAGE
Zeewolde, The Netherlands.

Overlay of master facets (blue) upon colour infrared videoframe.

20 GCP's
28 triangles

CARTOSCAN

Plate 6 Geometrical transformed colour infra-red image of Zeewolde village, as shown in plate 5. The overlay (blue) represents the Delauny facets based on the master coordinates. The pixels in plate 5 not enclosed by a triangle, were excluded from the transformation.

The National Remote Sensing Programme 1990-2000, (NRSP-2) is implemented under the responsibility of the Netherlands Remote Sensing Board (BCRS) and coordinated by the Ministry of Transport and Public Works.

The objectives of the NRSP-2 are: to secure the long-term integration of the operational use of remote sensing through temporary stimulation in the user-sectors of government and industry, to strengthen the development of remote sensing applications and the expansion of the national infrastructure.

Publication of:

Netherlands Remote Sensing Board (BCRS)
Programme Bureau
Rijkswaterstaat Survey Department

P.O. Box 5023
2600 GA Delft
The Netherlands
tel.: + 31 15 691111
Fax: 618962